On the Enigma of the Human Neurenteric Canal

Alexander Rulle[a]   Nikoloz Tsikolia[a]   Bernadette de Bakker[b]   Charis Drummer[c]
Rüdiger Behr[c, d]   Christoph Viebahn[a]

[a]Institute of Anatomy and Embryology, University Medical Center Göttingen, Göttingen, Germany; [b]Department of Medical Biology, Section Clinical Anatomy & Embryology, Amsterdam UMC, University of Amsterdam, Amsterdam, The Netherlands; [c]Platform Degenerative Diseases, German Primate Center, Leibniz Institute for Primate Research, Göttingen, Germany; [d]University Medical Center Göttingen, Göttingen, Germany

Abstract
Existence and biomedical relevance of the neurenteric canal, a transient midline structure during early neurulation in the human embryo, have been controversially discussed for more than a century by embryologists and clinicians alike. In this study, the authors address the long-standing enigma by high-resolution histology and three-dimensional reconstruction using new and historic histological sections of 5 human 17- to 21-day-old embryos and of 2 marmoset monkey embryos of the species *Callithrix jacchus* at corresponding stages. The neurenteric canal presents itself as the classical vertical connection between the amniotic cavity and the yolk sac cavity and is lined (a) craniolaterally by a horseshoe-shaped "hinge of involuting notochordal cells" within Hensen's node and (b) caudally by the receding primitive streak epiblast dorsally and by notochordal plate epithelium ventrally, the latter of which covered the (longitudinal) notochordal canal on its ventral side at the preceding stage. Furthermore, asymmetric parachordal *nodal* expression in *Callithrix* and morphological asymmetries within the nodes of the other specimens suggest an early non-cilium-dependent left-right symmetry breaking mode previously postulated for other mammals. We conclude that structure and position of the mammalian neurenteric canal support the notion of its homology with the reptilian blastopore as a whole and with a dorsal segment of the blastopore in amphibia. These new features of the neurenteric canal may further clarify the aetiology of foetal malformations such as junctional neurulation defects, neuroendodermal cysts, and the split notochord syndrome.
                                                © 2018 S. Karger AG, Basel

Introduction

Gastrulation is the life-shaping process of germ layer formation in the animal kingdom, its name being derived from the image of a "mini-stomach" transiently formed by the blastula (or blastocyst) stage embryo [Haeckel,

This paper is dedicated to the late Ronan O'Rahilly, who died in Fribourg, Switzerland, June 24, 2018, at the age of 96.

Christoph Viebahn
Institute of Anatomy and Embryology
Kreuzbergring 36
DE–37075 Göttingen (Germany)
E-Mail christoph.viebahn @ medizin.uni-goettingen.de

1874]. Germ layers are formed by cellular involution and delamination of the (outer layer) epiblast cells at the lips of a canal-like blastopore in amphibians and in reptiles (i.e., in non-avian or non-mammalian amniotes) such as turtles, lizards, and tuatara, the latter being thought to represent a common ancestor; alternatively, germ layers in mammals including *Homo sapiens* and birds are formed by cellular ingression and epithelial-mesenchymal transition at the primitive streak (with its anterior-posterior axis-defining furrow in the epiblast). Blastopore and primitive streak have, therefore, repeatedly presented to be functional equivalents derived from a common ancestor and thus to be homologous structures [Arendt and Nübler-Jung, 1999]. A recent focus on reptiles, however, led to the proposal that the avian and the human primitive streak may have developed independently and that reptiles with their narrow canal-like blastopore, which runs more or less perpendicularly through the embryonic plate connecting the amniotic cavity with the yolk sac cavity [Bertocchini et al., 2013], may have an "intermediate blastopore" or "proto-streak" with crucial importance for gastrulation [Stower and Bertocchini, 2017].

Early morphological studies of Kowalevsky in 1869 [Kowalevsky, 1877; Neuhauser and Kaufmann, 1961] on the spiny dogfish (*Squalus acanthias*) described a morphological structure similar to the reptilian and amphibian blastopore which penetrates perpendicularly all germinal layers and is closely related in terms of developmental time and localization to the emergence of the chorda dorsalis, the class-defining axial structure in the animal kingdom. Later, this transient blastopore-like structure was called the neurenteric canal and indeed assumed to be a homologue of the blastopore [Hoffmann, 1883] on account of the morphological similarity. Subsequently, the neurenteric canal was also observed during development of mammals such as *Vespertilio murinus* (the parti-coloured bat) immediately cranial to the primitive streak but caudal to the primitive (or Hensen's) node [van Beneden, 1888]. In human embryos, the neurenteric canal was described first by von Spee [1889] but considered by some as a post-mortem artefact [Sternberg, 1927] while other publications stated its appearance to be physiological [Odgers, 1941; O'Rahilly and Müller, 1981]. In fact, the controversy about the existence of the neurenteric canal during human development has never ceased, even when enforced by clinicians speculating about its role in foetal malformations [Holschneider and Fendel, 1971]. Human embryos of the stages in question (Carnegie stages 8 and 9; on average at 17–21 days of development) are rare, mostly dating back to the last century, and distributed worldwide in many embryological collections. However, embryologists always agreed on the definition of another transient canal-like structure with a dorsal opening to the amniotic cavity but appearing at slightly earlier stages: the notochordal canal or chorda canal [Grosser, 1924], which had been found first in the hedgehog and the guinea pig [Lieberkühn, 1882] and later also in a human embryo by Eternod [1899]. The notochordal canal is a longitudinal canal between the (epithelial cells of the) developing notochordal plate dorsally and mesenchymal cells of the axial mesoderm ventrally [van Beneden, 1888; Sternberg, 1927; Heuser, 1932]. This ventral stretch of the axial mesoderm was recently found also in the chick (where a typical notochordal canal has not been described so far) and was coined subchordal mesoderm (SCM) in contradistinction to the notochordal plate lying dorsal to it [Tsikolia et al., 2012]; its presence was soon confirmed in several mammalian species such as rabbit, pig, and cattle, and furthermore shown to be topographically related to an early non-cilium-dependent molecular left-right asymmetry [Schröder et al., 2016]. During further development in mammals, the notochordal canal loses its ventral wall as the SCM disintegrates through an as yet unknown mechanism with the effect that the notochordal plate has direct contact to the yolk sac cavity [Heuser, 1932]. Intriguingly, the process of SCM disintegration is suited to give rise to a dorsoventrally oriented canal remnant, which connects the amniotic cavity with the yolk sac cavity, may persist until early somite stages, and, therefore, fits the criteria of the neurenteric canal mentioned above [O'Rahilly and Müller, 1987]. However, the most recent descriptions in the human embryo, which took advantage of the few well-preserved specimens with signs of a neurenteric canal, only [Müller and O'Rahilly, 2003, 2004], still left some room for interpretation as to the terminology and definition for both the notochordal or a neurenteric canal in the human embryo.

Inspired by observations on (1) an unpublished human stage 8 embryo with excellent tissue preservation in the collection of the Center of Anatomy at the University of Göttingen and (2) two (stage 8 and 9) embryos of *Callithrix jacchus* (the common marmoset monkey), the authors address the enigma of the neurenteric canal anew, this time also including previous suggestions about the homology of its neighbouring structures in human and non-human primate embryos: On the basis of a clear definition of the cellular composition in the walls of the notochordal canal and the neurenteric canal during gastrulation of non-human primates and with reference to the "charnière de réflexion" [Pasteels, 1943] – later renamed

Table 1. Embryos investigated in this study

Species	Specimen No./name	Year of publication	Location	Carnegie stage	Fix.	Emb.	Sect. plane	Sect. thickn., μm	Stain	3DR
Human	93.2.2	2001[1]	CAG	8a	B	P	sag.	10	H&E	24 sect. 4 sect.[10]
Human	CC8671	1949[2]	CCW[7]	8a	A&B	C&P	sag.	6	H&E	30 sect. 6 sect.[10]
Human	Dobbin	1931[3]	NB	8b	Al	C&P	tr.	8	unknown	55 sect.
Human	CC10157	1967[4]	CCW[8]	8b	F	P	to	5–8	C	39 sect. 16 sect.[10]
Human	Da1	1928[5]	unknown	9	B	P	tr.	8	A	6 sect.
Callithrix jacchus	GM79.01	2018[6]	CAG[9]	8b	B	Te	tr.	5	H&E	65 sect.
Callithrix jacchus	GP09.01	2018[6]	CAG	9	B	P	tr.	7	H&E	34 sect.

3DR, three-dimensional reconstruction; B, Bouin; F, formaldehyde; A&B, alcohol and Bouin; Al, alcohol; P, paraffin; C&P, cedarwood oil-pyroxelene and paraffin; Te, Technovit; H&E, haematoxylin and eosin; C, Cason; A, Alaun-Cochenille; CAG, Center of Anatomy Göttingen; CCW, Carnegie Collection at Washington DC; NB, Naturkundemuseum Berlin; sag., sagittal; to, transverse oblique; tr, transverse.
[1] Sander [2001]. [2] Hertig and Gore [1966], O'Rahilly and Müller [2006] and de Bakker et al. [2016]. [3] Hill and Florian [1931]. [4] O'Rahilly and Müller [1987]. [5] Ludwig [1928]. [6] This study. [7] Sections available for download at http:/3datlas.3dembryo.nl/. [8] Cork and Gasser [2017a]; sections available at http://virtualhumanembryo.lsuhsc.edu/downloads/DREM_disks.html. [9] Analyzed by whole-mount in situ hybridization prior to histological sectioning. [10] Number of sections used for "wide" reconstruction mode (see Materials and Methods).

"chordoneural hinge" [Gont et al., 1993; Beck and Slack, 1998; Cambray and Wilson, 2002] – the histology of suitable human specimens previously published is re-interpreted and subjected to high-resolution three-dimensional reconstruction (3DR). As the results were also obtained in *C. jacchus,* which serves as a timely primate model organism from stem cell research [Thomson et al., 1996; Sasaki et al., 2005; Boroviak et al., 2015; Debowski et al., 2016] to virology [Greenough et al., 2005; Leibovitch et al., 2013], the data presented here may be translated to other non-human primates [Selenka, 1900; Heuser and Streeter, 1941; Hendrickx, 1971] and may in this larger context then further clarify, on the one hand, the mechanisms of human gastrulation and neurulation, and, on the other hand, the evolution of generating the amniote body plan.

Materials and Methods

The embryos studied in this publication are listed in Table 1 according to species and their classification in Carnegie stages. The 2 marmoset embryos of the species *C. jacchus* and the human specimen with the designation 93.2.2 belong to the collection of the Center of Anatomy in Göttingen (Germany). The other 4 human

embryos were analyzed on the basis of published data as indicated. Using the length of the notochordal plate as an established marker for the definition of stage 8 embryos, subdivisions between stage 8a (notochordal plate ventrally covered by SCM) and stage 8b (notochordal plate with direct contact to yolk sac cavity) were defined for a more precise classification.

Human Embryos
Embryo 93.2.2 had been accidently found at a medically indicated abrasio uteri in the year 1993, immersed in Bouin solution for several weeks starting 30 min after the operation, photographed in Locke solution, embedded in paraffin, serially sectioned sagittally at 10 μm, and stained with haematoxylin and eosin. The first histological description of the embryo was part of the medical dissertation by Sander [2001] who reconstructed the embryo using the projection method established by Gihr [1961]. The menstrual history of the mother, and thus the estimated development time, is unknown, but the embryo was categorized on morphological grounds as a Carnegie stage 8a embryo. The collection and use of this embryo in the present study was approved by the Ethics Committee of the University Medical Center Göttingen under reference No. 28/2/18An.

The human embryos CC8671 (stage 8a) [Hertig and Gore, 1966] and CC10157 (stage 8b) belong to the Carnegie Collection in Washington D.C. [O'Rahilly and Müller, 1987]. Details of their processing is listed in Table 1. Images and the necessary technical data of these 2 specimens were either available through open-source sites [Cork and Gasser, 2017a] or publications [de Bakker

Rulle/Tsikolia/de Bakker/Drummer/Behr/Viebahn

et al., 2016]. Unfortunately, the numbering of the sections of embryo CC10157 proved to be inconsistent since the "section number" and the "section location (slide number)" [Cork and Gasser, 2017c] are given in ascending and descending order, respectively. As a consequence, the left-right orientation of the embryo cannot be determined on the basis of the series of histological sections alone (see Results) but had to follow previous reconstructions [Cork and Gasser, 2017c]. The embryo "Dobbin" (Carnegie stage 8a) had been fixed after abortion and estimated to be recovered at 17 days post coitum (dpc) [Hill, 1931]; the histological sections are part of the collection of the Naturkundemuseum in Berlin, Germany. Embryo "Da1" (Carnegie stage 9 and estimated to be recovered at 21 dpc) had been found intraoperatively during a tubal sterilization [Ludwig, 1928]. It was registered last at the collection of the Institute of Anatomy of the University of Basel, but its current location is unknown.

C. jacchus *Embryos*

All animals used in this study were handled in accordance with the German Animal Protection Act (Deutsches Tierschutzgesetz) as described previously by Aeckerle et al. [2015]. Specifically, the collecting of *C. jacchus* embryos was approved under the license No. 42502-04-12/0708 at the Lower Saxony State Office for Consumer Protection and Food Safety in Oldenburg, Germany. Animals originate from the self-sustaining *C. jacchus* colony of the German Primate Center (Deutsches Primatenzentrum) in Göttingen. One embryo donor (#14457) was 6 years and 5 months old at the time of sacrifice. The other one (#12944) was 7 years and 10 months old. Embryo donors were euthanized by intracardial injection of 0.5–1.0 mL Narcoren® (160 mg/mL pentobarbital; Merial GmbH, Hallbergmoos, Germany) in deep anaesthesia (0.05 mL diazepam, 0.05 mL/100 g body weight "Göttinger Mischung II," applied intramuscular) prior to hysterectomy performed by an experienced veterinarian. Uteri were immersed in phosphate-buffered saline solution (PBS) at room temperature and the decidua was exposed as a whole by opening the peri- and myometrium as one unit using iridectomy scissors. Embryos were dissected by careful blunt separation of the intact decidua, photographed, and immediately fixed in 4% paraformaldehyde in PBS at room temperature. Embryonic staging was carried out on the basis of the morphological criteria of the Carnegie staging system for human embryos [O'Rahilly and Müller, 1987] using dark field microscopy. The embryos were collected primarily for germ cell studies (see license No. 42502-04-12/0708) [Aeckerle et al., 2015]. Parts of the embryos not required for this purpose were used for this study and subjected to different embedding protocols after dissection: embryo GM79.01 (recovered at 46 dpc and classified as stage 8b) was dehydrated in a graded series of ethanol and stored in ethanol at –20 °C until its later use for whole-mount in situ hybridization (WISH, see below), after which Technovit® 8100 (Heraeus Kulzer GmbH, Wehrheim, Germany) served as embedding medium for high-resolution histology and cellular localization of *nodal* mRNA expression as described previously [Schröder et al., 2016]. Sections (5 μm) were transferred in pairs onto glass slides and a few glass slides were used for test staining (their WISH staining reaction remaining accidentally unphotographed) to identify the staining technique which would enable easy identification of cellular borders and thus detailed 3-dimensional reconstruction (3DR) afterwards (s.b.). Except for these test slides, sections were photographed using differential interference contrast without counter-staining to visualize the staining reaction after WISH for *nodal* mRNA expression. After the WISH staining reaction was thus digitally recorded, all glass slides of GM79.01 underwent haematoxylin-eosin staining according to Gill for 20 min, which then obscured the *nodal* expression domain. Embryo GP.09.01 (recovered at 49 dpc and classified as stage 9) was fixed in Bouin solution (30% picric acid, 30% acetic acid, 4% formaldehyde in PBS), embedded in paraffin wax, and serially sectioned at 7 μm. The sections were placed on slides and stained with Harris haematoxylin for 1.5 min and eosin for 5 min [Bancroft and Layton, 2013].

Whole-Mount in situ Hybridization

The *C. jacchus nodal* cRNA probe was generated by in vitro transcription from PCR products of a cDNA template. In situ hybridization was performed according to the protocol described previously by Püschel and Jouneau [2015]. In short, the cryofixed specimen (100% ethanol at –20 °C) was rehydrated and treated with proteinase K for 15 min to guarantee infiltration of the *nodal* probe at the subcellular level, refixed for 20 min in 0.2% glutaraldehyde/PBS with Tween, followed by 1 h of pre-hybridization at 70 °C in hybridization buffer (formamide, saline sodium citrate buffer [pH 4.5], 0.5 mM EDTA, 10 mg/mL tRNA, 0.2% Tween 20, 10% CHAPS, and 50 mg/mL heparin). Subsequently, hybridization with 1 μL digoxigenin-labelled cRNA denatured at 95 °C was performed overnight at 70 °C. Excess cRNA was washed off using hybridization buffer and maleic acid buffer (100 mM maleic acid, 150 mM NaCl, 0.1% Tween 20 [pH 7.5]) prior to blocking unspecific antibody binding sides using maleic acid buffer with 2% Boehringer blocking reagent (Roche, Mannheim, Germany) and 20% heat-inactivated goat serum. Alkaline phosphatase-linked anti-digoxigenin antibody (Roche) was added, the specimen stored at 4 °C for 12 h, and the surplus antibody eluted with maleic acid buffer. The colour reaction with BM-purple substrate (Roche) lasted 4 days at room temperature in the dark and was stopped using alkaline phosphatase buffer (NTMT: 100 mM Tris, 100 mM sodium chloride, 50 mM magnesium chloride, 2 mM levamisole, 0.1% Tween 20) followed by PBS. Finally, the embryo was embedded in Mowiol® (Hoechst, Frankfurt, Germany) for whole-mount photography and processed for Technovit® embedding as described above.

Three-Dimensional Reconstruction (3DR)

Image acquisition was carried out with a Zeiss Axioplan 2 microscope and Zeiss AxioCam MRc resulting in red green blue (RGB) tagged image file format (TIFF) files at a resolution of 1,388 × 1,040 pixels. Section photographs, either viewed from left (for sagittal sections) or from caudal (for transverse sections), were aligned and digitally segmented manually with the open-source program "Fiji-ImageJ-win64" and its plugin "TrakEM2" [Schindelin et al., 2012]. The x- and y-axes were adjusted (a) according to the known μm/pixel ratio of the camera used (for 93.2.2; Dobbin; CC10157; GM79.01; GP09.01) or (b) according to an estimate of the μm/pixel ratio using measurements of published data (see O'Rahilly and Müller [2006] for CC8671 and Ludwig [1928] for Da1). Colours were applied independently from the ones found at source (own photographs, internet, publication) as follows: blue for neurectoderm, red for mesoderm, green for basement membrane, and purple for notochordal plate. In embryo GM79.01 beige was used for the area of *nodal* expression; *nodal* segmentation had to be interpolated for those few sections in which the WISH signal

was obscured by the counterstaining before the 3DR had been carried out.

Two methods of reconstruction (called "narrow" and "wide," respectively) were established to give consideration to the fact that some structures of interest were smaller than the section thickness [for further explanations, see the online supplementary information (see www.karger.com/doi/10.1159/000493276 for all online suppl. material)]. As a general quality check, all reconstructions were compared to pre-sectioning stereo-microscope images or published reconstructions with regard to size and shape of "macroscopic" features such as the overall shape of the embryonic disc or morphological left-right asymmetry. If necessary, adjustments were made by realignment of the sections. Adobe Acrobat Pro (www.adobe.com) was used for creating 3D-PDF files (available in the online suppl. material). Using the software "MakerBot print" and the 3D printer "MakerBot replicator$^+$" (www.makerbot.com), a physical 3D model of the central embryonic disc region of GM79.01 and measuring $10 \times 6 \times 3$ cm was created.

Results

Morphology of Human Embryos

The new human stage 8a embryo available for this study (designation 93.2.2) has an elongated embryonic disc which measures 1.1×0.9 mm (see Fig. 1a, taken from Sander [2001]), displays a short allantois and separates 2 voluminous cavities: the yolk sac and the amniotic cavity. In the dorsal view of the reconstruction (Fig. 1a), the anterior-posterior axis is marked by a narrow thickening measuring 0.3 mm in length which is caused by the developing notochord; the future cranial pole of the embryo is marked by the anterior extremity of the notochord while the future caudal pole is marked by the posterior attachment of the notochord to the primitive node, the latter being remarkably inconspicuous in this specimen. The serial sagittal paraffin sections through the embryonic disc confirm the longitudinal S-shaped configuration of

the germ layers with the (dorsal) neuroectodermal layer consisting of cylindrical cells near (Fig. 1c, e, f) and within (Fig. 1d, g) the median plane and continuing anteriorly and laterally in the cuboidal cell layer of the epidermal ectoderm. At the anterior and lateral borders of the embryonic disc, the row of cuboidal ectoderm cells bends dorsally and is connected – without a definite border – to the squamous epithelium of the amnion. High magnification (Fig. 1g) reveals subcellular details in the neuroectoderm such as (a) nuclei which are large relative to the cytoplasmic volume and which have distinct nuclear membranes and nucleoli, (b) apically placed "mitotic figures" from various stages of mitosis (Fig. 1e), (c) differentiation of low-density cytoplasmic sub-regions either apical or basal to the interphase nuclei indicating a high degree of vacuolization, and (d) an almost continuous line basally representing the position of the basement membrane. Ventrally adjacent to the neuroectoderm lies the notochord which consists of an inverted simple epithelium with basally positioned nuclei (i.e., close to the basement membrane of the neuroectoderm) and cytoplasmic sub-regions of low density positioned towards the apical extremities of the cells (Fig. 1g). The basal row of cell nuclei of the notochord epithelium is also visible in parasagittal sections (Fig. 1c, e, f) and continues cranially furthest in the median plane, where it touches the irregularly arranged prechordal mesoderm cells near the dorsal bend of the neuroectoderm (Fig. 1b). In its midline position, the simple epithelium of the notochord forms the dorsal part of the axial mesoderm and it is ventrally covered by a mesenchymally differentiated part of the axial mesoderm which is characterized by numerous small cells and a stochastic positioning of cell nuclei (Fig. 1g). In its position ventral to the notochordal epithelium and due to its caudal continuation with the mesodermal cells of the

Fig. 1. Human stage 8a embryo (specimen No. 93.2.2). **a** Dorsal view of the 3D reconstruction in Sander [2001]: 1, cut edge of the opened amniotic cavity; 2, notochord; 3, proximal rim of the opened yolk sac. C–F, position of sections shown in **c–f**. **b** Low magnification of the median section shown in **d** displaying the bent embryonic disc (borders marked by black asterisks). **c–f** Left paramedian (**c**), median (**d**), and right paramedian (**e, f**) sagittal sections (section numbers indicated at the bottom left) at higher magnification. Blue box marks the area shown at high magnification in **g**. Black circle with line attached is centred on (the median part of) the hinge of involuting notochord cells. **g** High magnification of the area marked in **d** displaying the cellular composition of the neuroectoderm (blue square bracket), notochordal plate (purple square bracket), subchordal mesoderm (red square bracket), hypoblast (yellow square bracket), and notochordal canal (curved bracket). Black arrow marks the dorsal opening of the notochordal canal, black cross marks the caudal-most notochordal plate cell at the transition between neuroectoderm and notochordal plate. **h** Left lateral view of a "wide" semitranslucent reconstruction using 8 sections. Colour coding as used in **g**; green marks the basement membrane, black arrow and black cross markings as in **g**. A transition zone between neuroectoderm and notochordal plate is highlighted by an intermediate colour (blue-purple) between blue (for neuroectoderm) and red-purple (for notochordal plate). **i** Right dorsal semitransparent view of a "narrow" reconstruction, depicting the whole size of the notochordal plate (purple). Colours as in **g**. **j** Dorsal view of a "narrow" reconstruction. Scale bar: **a** 650 μm. **b** 300 μm. **c–f** 100 μm. **g** 50 μm.

(For figure see next page.)
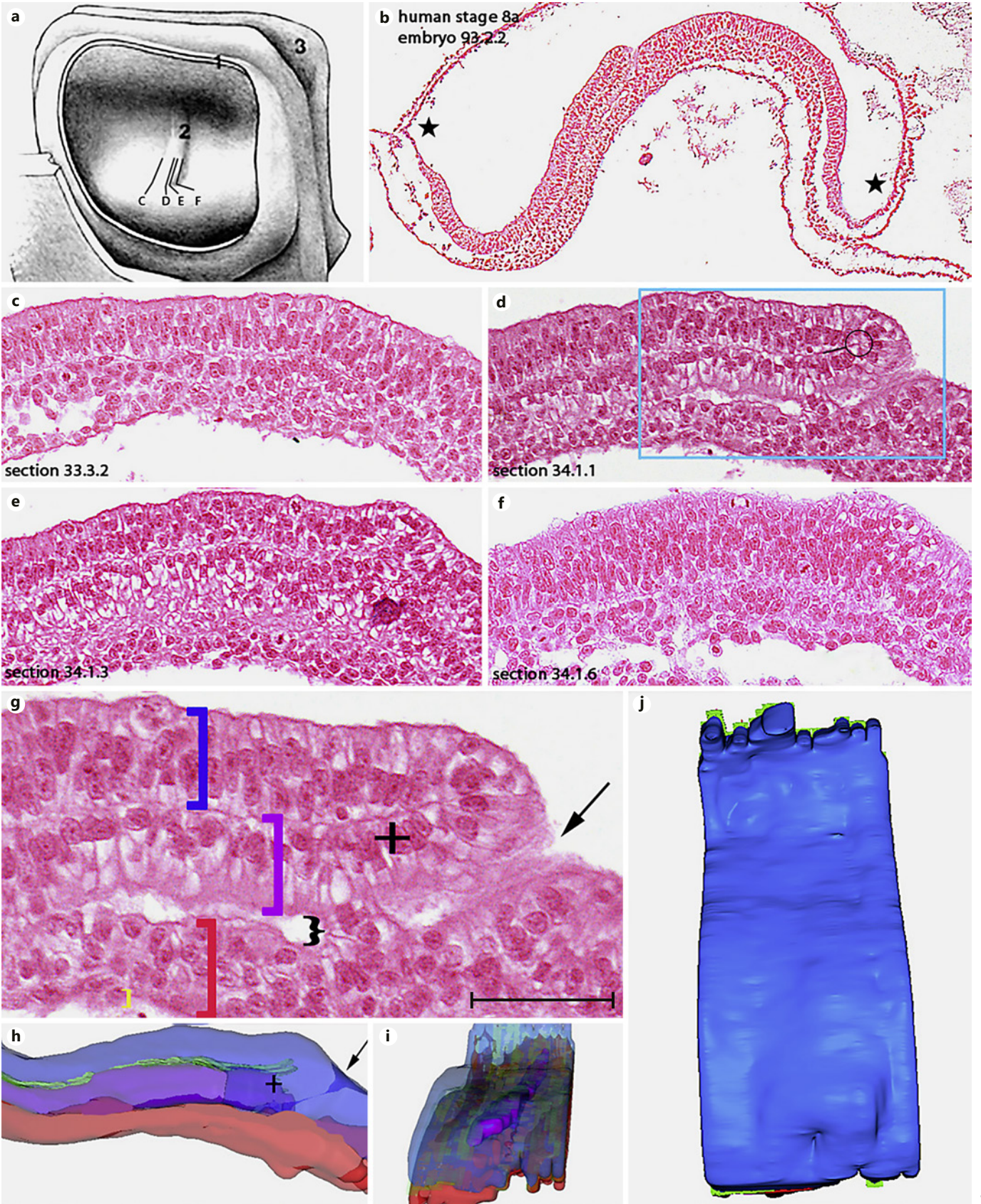
primitive streak, this mesenchymal axial mesoderm will be addressed here as SCM in accordance with observations made in the chick [Tsikolia et al., 2012] and several non-primate mammals [Schröder et al., 2016]. The SCM itself is covered – similar to the primitive streak mesoderm further posteriorly – by a single layer of squamous hypoblast cells (Fig. 1g) which continues laterally as yolk sac epithelium (not shown). In its caudal third, the epithelial part of the notochord is separated from the SCM by several narrow translucent extracellular spaces which are connected to each other by somewhat narrower semitranslucent extracellular spaces; taken together these spaces measure 180 μm in length, 10 μm in width, and 10 μm in height. Towards the cranial extremity of the notochord epithelium, this extracellular space tapers out, but caudally, in contrast, the clear extracellular space is connected to the amniotic cavity by a further stretch of semitranslucent extracellular space, which shows honeycomblike structures indicating the apical cortex of tangentially sectioned epithelial cells in the lateral wall of this dorsal opening to the amniotic cavity (Fig. 1g).

At the caudal end of the neuroectodermal basement membrane, both neuroectoderm and notochordal epithelium are connected by epithelial cells which are radially arranged and tend to have their cell nuclei positioned basally; their apical surfaces are in contact serially with the amniotic cavity dorsally and the semitranslucent extracellular spaces ventrally. This arrangement is typical for an epithelial sheet undergoing involution around a hinge which presents itself as a narrow point in sections through the median plane (Fig. 1e) and may continue laterally to form a broader ledge. Posterior to the cranial rim of the primitive node a distinct primitive pit typical for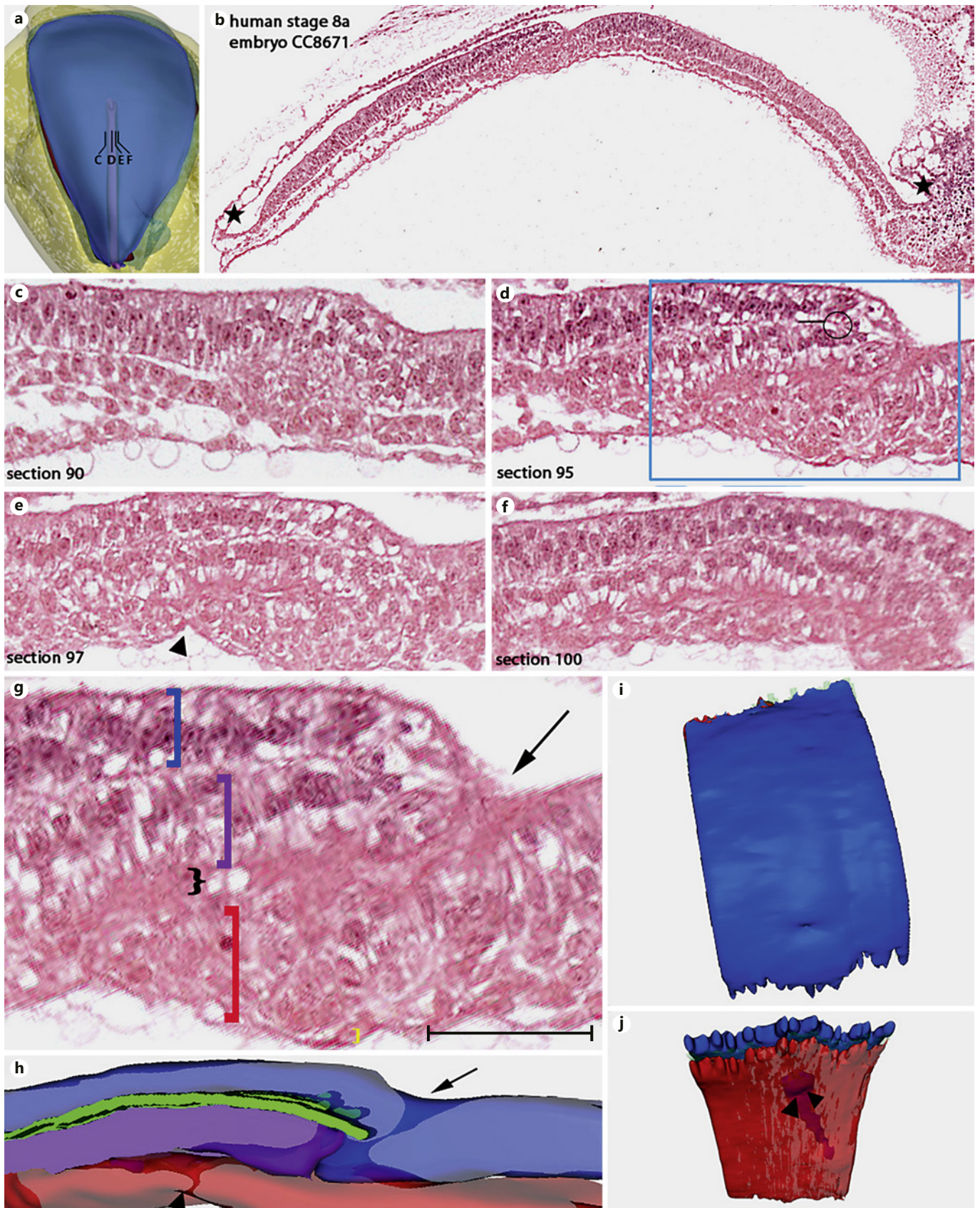 most non-rodent mammalian embryos [Hensen, 1876] is seen in this specimen (Fig. 1b); the conspicuous radial arrangement of epithelial cells within the cranial rim of the node is therefore addressed here as hinge of involuting notochordal cells (HINC) in accordance with the terminology on cell movement during gastrulation summarized by Gilbert and Barresi [2016]. With this definition, HINC is principally different from the "chordoneural hinge" of Pasteels [1943], Gont et al. [1993], and Cambray and Wilson [2002], because the latter is an area of proliferating cells for both neuroectoderm and axial mesoderm during secondary neurulation either in the late dorsal blastopore lip (of amphibia) or the tail bud (in amniotes), respectively. As a further conspicuous feature of the specimen 93.2.2, the right side of the primitive node is higher, and the nuclei are more frequently round and arranged in more layers than on the left side (cf. Fig. 1c, f). Therefore, both these lateral parts of the primitive node will be addressed as "node shoulders" in analogy to the situation found in the chick [Tsikolia et al., 2012].

The (dorsal) epithelial part of the notochord gives the notochord a plate-like shape extending from the HINC at its caudal extremity to the prechordal mesoderm at its cranial extremity. This homogeneous epithelial differentiation in contradistinction to the underlying SCM is the basis for addressing the notochord in the description of this and the following stages as the "notochordal plate." This encompassing definition used here facilitates (1) the identification of dorsal and ventral parts of the axial mesoderm prior to the intercalation of the dorsal wall of the notochordal process into the endoderm and prior to the formation of the notochordal canal, (2) addressing the extracellular spaces between dorsal and ventral parts of the axial mesoderm as a notochordal canal still intact (in accordance with the original description by Lieberkühn

Fig. 2. Human stage 8a embryo (specimen No. CC8671; section images obtained at: http:/3datlas.3dembryo.nl/). **a** Dorsal view of the 3D reconstruction in de Bakker et al. [2016] displaying primitive streak (purple), proximal rim of yolk sac (yellow), and embryonic disc (blue) with cut edge of amnion. C–F indicate section planes shown in **c–f**. **b** Low magnification of section 95 shown in **d** displaying the straight embryonic disc (borders marked by black asterisks). **c–f** Left paramedian (**c**), median (**d**), and right paramedian (**e**, **f**) sagittal sections (section numbers indicated at the bottom left) at higher magnification. Blue box marks the enlarged area shown in **g**. Black circle with attached line is centred on (the median part of) the hinge of involuting notochord cells. Black arrowhead in **e** marks the ventral indentation of the hypoblast as an indication of an open connection developing between the notochordal canal and the yolk sac cavity. **g** High magnification of the area marked in **d** displaying the cellular composition of neuroectoderm (blue square bracket), notochordal plate (purple square bracket), subchordal mesoderm (red square bracket), hypoblast (yellow square bracket), and notochordal canal (curved bracket). Black arrow marks the dorsal opening of the notochordal canal. **h** Left lateral view of a "wide" semitranslucent reconstruction using 6 sections. Colours as in **g**; green marks the basement membrane. Black arrowhead marks the ventral hypoblast indentation as a potential ventral opening of the notochordal canal, black arrow marks its dorsal opening. **i** Dorsal view of a "narrow" reconstruction showing the neuroectoderm with the dorsal opening of the notochordal canal and the oblique course of the notochordal plate. **j** Ventral view of a narrow reconstruction showing the whole length of the notochordal plate. Black arrowheads mark the positions of the ventral indentations as potential openings of the notochordal canal. Scale bar: **a** 880 μm. **b** 330 μm. **c–f** 100 μm. **g** 50 μm.

(For figure see next page.)

b human stage 8a embryo CC8671

section 90

section 95

section 97

section 100

2

[1882] and previous descriptions in early stage 8 human embryos [Strahl, 1916; Rossenbeck, 1923; O'Rahilly and Müller, 1981]), and (3) describing the transition of the caudal part of the notochordal canal into the neurenteric canal by local disintegration of the SCM (see van Beneden [1888] and O'Rahilly and Müller [1981], and below).

In 3DRs, the following 4 morphological characteristics become apparent as the salient structures surrounding the notochordal canal. Firstly, the dorsal opening of the notochordal canal is recognized in the region of the primitive node to be completely surrounded by epithelial cells, while the notochordal canal is visible between the notochordal plate and the SCM (Fig. 1h). Secondly, the node rises from left to right and has a steep "descend" lateral to the right shoulder (Fig. 1j), and the basement membrane in the area of the node just anteriorly and laterally of the canal, where the epithelium involutes, and under the right half of the notochordal plate (Fig. 1i). Thirdly, the notochordal plate runs diagonally from posterior-left to anterior-right, even though the sectioning axis diverges – in this part of the embryo – from the longitudinal axis of the embryo to the left. The first epithelial cells standing perpendicularly on the basement membrane after turning by 180° through the HINC were hereby defined as the cranial transition point between neuroectoderm and notochordal plate, and this is indicated by a colour change from blue (for neuroectoderm) to purple (for notochordal plate; see Fig. 1g, h). Finally, the primitive streak – identified by a missing basement membrane and a dorsal groove in the epiblast epithelium – forms with its (epithelial) epiblast cells the ventro-caudal wall of the dorsal opening of the notochordal canal.

The embryonic disc of the second human stage 8a embryo (designation CC8671) was in toto reconstructed by de Bakker et al. [2016: Fig. 2a] its preservation status being deemed excellent [O'Rahilly and Müller, 1987]: it is pear-shaped and 1.38 mm long (Fig. 2b, see O'Rahilly and Müller [2006]). The primitive streak together with the notochordal plate indicates the orientation of the anterior-posterior axis which diverges from the longitudinal axis of the sagittal sections (Fig. 2c–f) by about 10° to the left. A distinct primitive pit is visible caudally adjacent to the primitive node and continues as a canal (measuring 145 μm in length, 40 μm in width, and 6 μm in height) between the developing notochordal plate and the SCM when examined in median histological sections (Fig. 2d, g). This canal-like structure is composed of occasional clear extracellular spaces and dense areas displaying honeycomb-like structures of apical cell membranes cut tangentially while its dorsal and ventral walls show identical cellular arrangements and subcellular structures as the notochordal canal in the embryo 93.2.2 (see above). Similarly, the neuroectoderm shows apically arranged mitotic figures and low-density subcellular regions apically and basally of interphase nuclei as in the embryo 93.2.2, and the HINC, too, is recognizable as the transition between neuroectoderm and notochordal plate within the cranial rim of the primitive node. Taken together, these histological features are the basis for addressing this canal-like structure as a shorter version of the bona fide notochordal canal described for 93.2.2.

Remarkably, the hypoblast layer shows 2 ventral indentations protruding into the adjacent SCM (Fig. 2e). With reference to the increasingly regressing ventral wall of the notochordal canal during Carnegie stage 8 [cf. O'Rahilly and Müller, 1987], these indentations are addressed as incipient connections of the notochordal canal with the yolk sac cavity. However, on the basis of the length of the notochordal process, this embryo is considered to be less advanced in development than the specimen 93.2.2 in which similar indentations of the hypoblast are not found (cf. Fig. 1d).

Fig. 3. Human stage 8b embryo (specimen name "Dobbin"). **a** Dorsal view of the 3D reconstruction in Hill and Florian [1931] displaying the notochord, primitive streak, cut edge of amnion, and proximal parts of the yolk sac. B, D, F, and H indicate the position of the transverse sections shown in **b–h** (section numbers indicated at the bottom left). **b, c** Cranial transverse section illustrating the closed notochordal canal in its cranial half at low (**b**) and high (**c**) magnification (note the wide bilateral artefactual extracellular space between neuroectoderm and mesoderm). **d, e** Transverse section through the posterior extremity of the notochordal plate illustrating the ventral opening of the neurenteric canal. Black circle with line attached marks the presumed position of the hinge of involuting notochord cells in the lateral wall of the neurenteric canal. Black arrowhead marks the ventral opening of the neurenteric canal. **f, g** Transverse section next to the section shown in **d** and **e** displaying the dorsal opening of the neurenteric canal (black arrow). **h** Transverse section through primitive streak forming the caudal wall of the neurenteric canal. **i** Dorsocaudal view of a "narrow" reconstruction using 55 sections displaying the dorsal surface of the ectoderm. **j** Ventral caudal view of a "narrow" reconstruction displaying the ventral openings of the neurenteric canal and the notochordal canal (black arrowheads). **k** Caudodorsal view of a "narrow" semitranslucent 3D reconstruction using 55 sections and displaying the dorsal opening of the neurenteric canal (black arrow) and its course through the embryonic disc (black square bracket). Scale bar: **a** 1 mm. **b, d, f, h** 300 μm. **c, e, g** 100 μm.

(For figure see next page.)

Rulle/Tsikolia/de Bakker/Drummer/Behr/
Viebahn

3
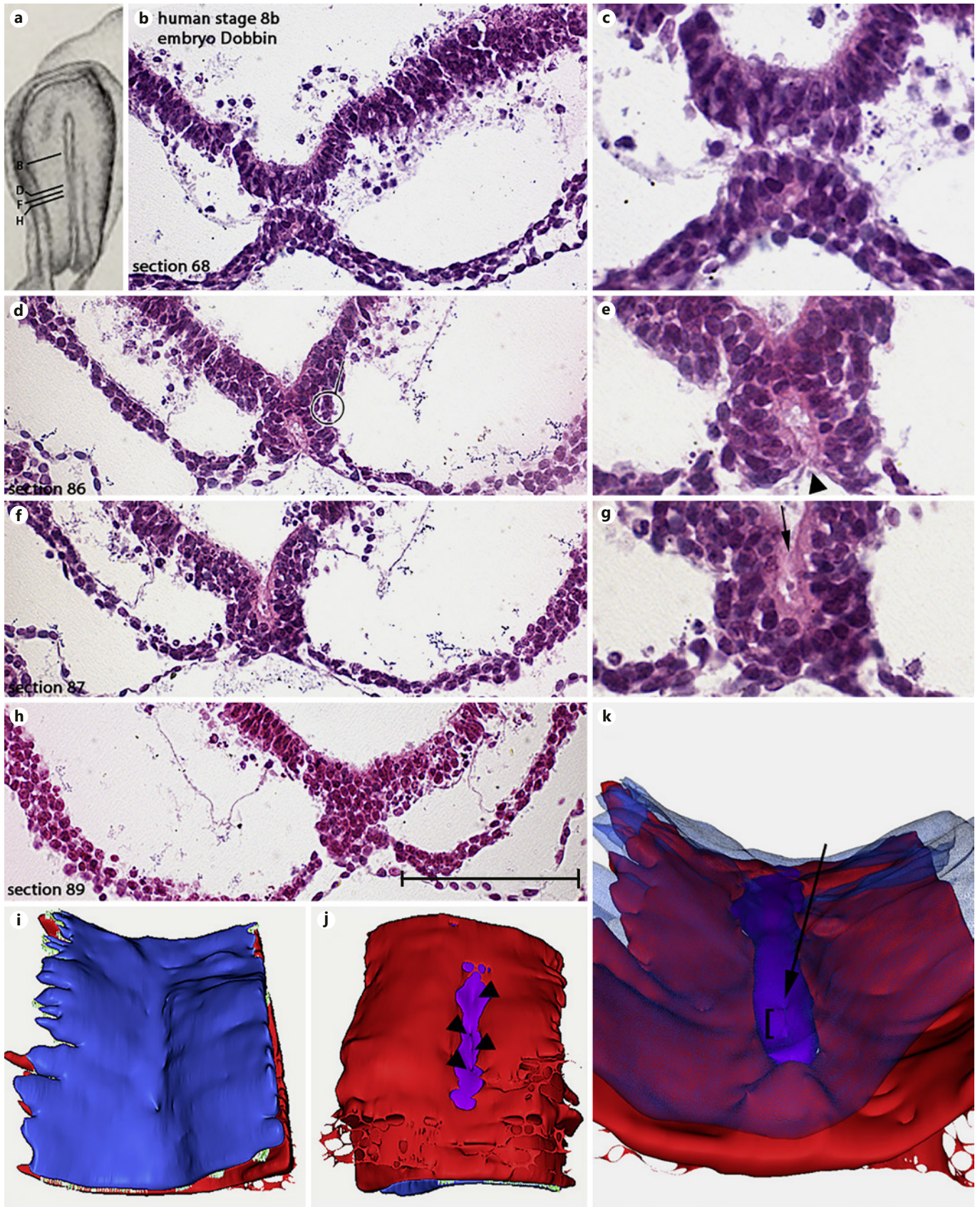
To the left side of the primitive node, the ectoderm is elevated mainly due to the bulging of the SCM which covers the notochordal plate ventrally at the level of the HINC and displaces the ectoderm towards the dorsal surface (Fig. 2c). The epithelium itself is almost symmetrical and contains oval nuclei on either side (Fig. 2c–f). Also, in the 3DR, the ectoderm appears symmetrical, which is apparent despite the oblique course of the notochordal plate (Fig. 2i). The dorsal opening of the notochordal canal is seen in the lateral view of a "wide" reconstruction (see results below, Fig. 2h), as is the ventral hypoblast indentation into the SCM just anterior to the primitive node (Fig. 2j).

Of the two human stage 8b embryos analyzed in this study, the embryo "Dobbin" (first description by Hill and Florian [1931]) is still pear-shaped and about 0.98 mm long from the anterior margin of the embryonic disc to the cloacal membrane (Fig. 3a). The cellular borders and intracellular organelles are difficult to identify in the histological sections due the poorer quality of tissue preservation than of the specimens described above; apical low-density cytoplasmic regions and apical cell contacts, however, are discernible as, for example, in some cells lining the notochordal canal (Fig. 3e). Inside the caudal extremity of the notochordal process (which measures 360 μm in length; Fig. 3b), a patent canal is seen running almost vertically through all 3 germ layers (Fig. 3d–g). As this embryo was serially sectioned in the transverse plane, the canal displays (1) a dorsal opening (measuring 6 × 4 μm) in the caudal-most section (Fig. 3f, g), (2) an almost complete ventral opening in the cranial-next section (Fig. 3d, e), and (3) a continuation in a central position in several sections further cranially (Fig. 3b, c). In its central position within the notochordal process, the canal is lined dorsally by the notochordal epithelium (notochordal plate) and ventrally by the irregular arrangement of SCM cells (Fig. 3c). In this way, the notochordal canal contin-

ues as a longitudinal canal in the anterior half of the notochordal process with a length of about 280 μm and can, therefore, be addressed as a notochordal canal running longitudinally within the notochordal process as described above for the stage 8a embryos. The part of the canal which is running vertically, however, is addressed as a bona fide neurenteric canal – running from caudodorsal to cranioventral – as originally defined in the human by von Spee [1889], Grosser [1924], and lately by O'Rahilly and Müller [1987]. As will be seen in the 2 other human embryos (stage 8b: Fig. 4; stage 9: Fig. 5) and in the non-human primates described below (Fig. 6, 7), this vertical canal is lined by epithelial cells laterally which are connected dorsally with the neuroectoderm by cellular arrangements (Fig. 3d, e) closely resembling the HINC described in the median plane in the 2 stage 8a human embryos (Fig. 1g, 2g). The transverse sections of this specimen, therefore, facilitate the definition of the HINC in the lateral walls of the dorsal opening of the neurenteric canal (Fig. 3d) which turn the median ledge-shaped HINC into a horseshoe-shaped area of involution. Furthermore, the transverse sections show the incipient intercalation of the ventral opening into the hypoblast (Fig. 3e). In the next section further caudally (Fig. 3g), the canal is seen to be limited by cells connected to the primitive streak (Fig. 3h) whereby the transverse orientation of the sections precludes a definition of these cells in the caudal wall of the neurenteric canal as epithelial versus mesenchymal.

Interestingly, the right side of the ectoderm immediately cranial to the dorsal opening of the neurenteric canal nearly doubles the left side in height and amount of nuclei (Fig. 3b). This leads to a bulging of the right parachordal ectoderm in the 3DR measuring about 120 μm in length (Fig. 3i). The 3DRs also show that the neurenteric canal lies immediately posterior to the primitive node (Fig. 3i, k). Caudally, the appearance of bottle cells under-

Fig. 4. Human stage 8b embryo (specimen No. CC10157). **a** Dorsal view of a reconstruction created by Cork and Gasser [2017c] indicating the embryonic disc borders (cut edge of the amnion) and the proximal rim of the yolk sac. B–F indicate the position of transverse sections shown in **b–f** (section numbers are taken from Cork and Gasser [2017c] and are indicated at the bottom left). **b** Transverse section showing the cranial end of the notochordal plate. **c** Transverse section through the posterior part of the notochordal plate showing lateral asymmetry in the neuroectoderm. **d** Transverse section containing the dorsal opening of the neurenteric canal (black arrow) and hinge of involuting notochord cells in the lateral wall of the neurenteric canal (black circle with line at-

tached). **e** Transverse section containing the ventral opening of the neurenteric canal (black arrowhead). **f** Transverse section through the centre of primitive streak. **g** Dorsal view of a "narrow" 3D reconstruction indicating the dorsal surface of the ectoderm. **h** Caudal view of a "wide" semitranslucent 3D reconstruction using 16 sections and indicating the course of the neurenteric canal. Black arrow marks the dorsal opening of the neurenteric canal. **i** Ventrocaudal view of a "wide reconstruction" displaying the ventral cone of the notochordal plate surrounding the ventral opening of the neurenteric canal. Black arrowhead marks the ventral opening of the neurenteric canal. Scale bar: **a** 800 μm. **b–f** 100 μm.

(For figure see next page.)

Rulle/Tsikolia/de Bakker/Drummer/Behr/
Viebahn
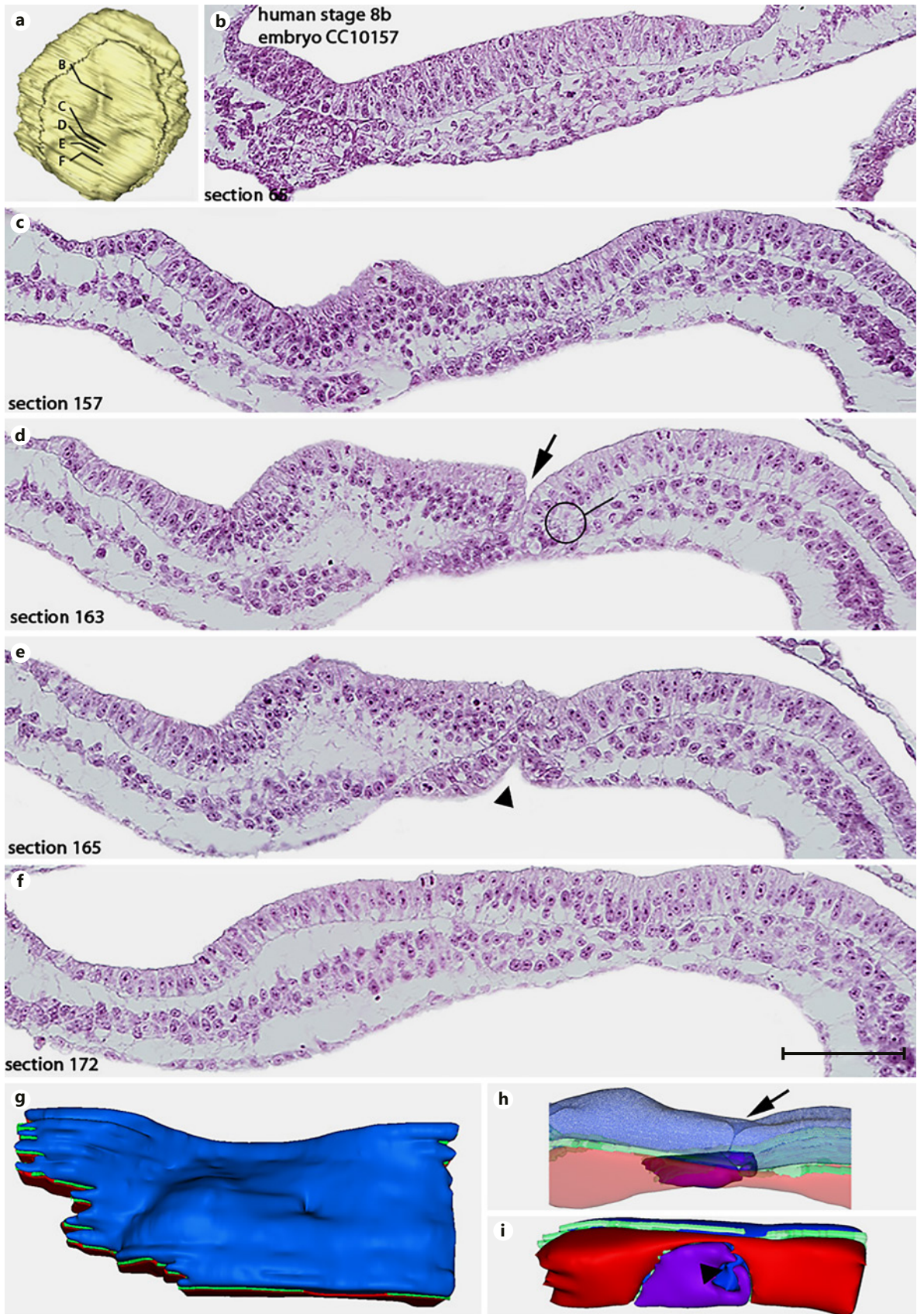
going epithelial-mesenchymal transition indicates the cranial-most (epithelial) epiblast cells of the primitive streak which are intercalated medially into the notochordal plate domain at the caudal border of the neurenteric canal. The posterior aspect of the neurenteric canal is surrounded dorsally by epiblast cells (coloured blue) and ventrally by notochordal cells (coloured purple in the 3DR). By taking the HINC as a regular wall structure into account, the neurenteric canal is thus shown to be surrounded by epithelial cells in its entire circumference (Fig. 3k). The ventral indentations in the SCM which may form openings of the longitudinal canal under the notochordal plate at later stages are visible when looking at the caudal aspect of the 3DR (Fig. 3j).

The other human stage 8b embryo analyzed in this study (designation CC10157; with excellent preservation according to O'Rahilly and Müller [1987]) has a large oval embryonic disc measuring 1.16 mm in its greatest diameter and is likely to possess a preparation artefact as stated by Cork and Gasser [2017b]. However, the region around the primitive node seems to be well preserved and suitable for high-resolution morphological analysis (Fig. 4a). Taking into account that the sectioning axis deviates from the transverse axis by about 20° clockwise to the right, a narrow and oblique canal between the amniotic and yolk sac cavity visible in 3 consecutive sections through the node area (Fig. 4d, e) can be defined to run almost perpendicularly from the cranial-right to the caudal-left and to have a diameter of 4 μm. The canal is addressed as a bona fide neurenteric canal also because it is lined laterally by epithelial cells (Fig. 4d, e) which are connected to the neuroectoderm through a HINC (see Fig. 4d) as in the embryo Dobbin (Fig. 3d). In comparison to this embryo, however, there is a wider zone of ventral columnar-epithelial cells intercalated into the hypoblast and forming a cone surrounding the ventral opening of the neurenteric canal; this is similar to the situation found in the stage 8b *Callithrix* specimen described below (Fig. 6, 7). The columnar-epithelial cells of this cone are found caudal and lateral (fig. 4e; to the right) as well as cranial and lateral (Fig. 4e;

to the left; Fig. 4d; to the left) to the neurenteric canal and, further cranially, connect to the broad notochordal plate intercalated into the hypoblast (Fig. 4c); caudally they are attached to the adjacent primitive streak (Fig. 4f). Altogether, the notochordal plate is 650 μm long, and the apical surface of its epithelial cells has a direct connection to the yolk sac cavity (Fig. 4c). At the very cranial end of the notochordal plate, a cluster of cells with an irregular arrangement form the anterior-most part of the notochord (Fig. 4b) and contains several extracellular cavities which resemble the remains of a notochordal canal although the latter is not clearly definable in this embryo. However, the length and width of the notochordal plate and the absence of a clear notochordal canal gives this embryo a more advanced appearance than the 2 other stage 8b embryos described in this study. According to the left-right orientation given on the digital source of this series of sections [Cork and Gasser, 2017c], it is the left parachordal ectoderm which presents itself as a thickened epithelium near the primitive node. Its cells form multiple layers of cuboidal cells over a length of 130 μm (Fig. 4c).

In 3DRs, too, the left parachordal ectoderm appears markedly elevated (Fig. 4g); the lack of a basement membrane in its centre is most likely due to its artificial dislocation into an oblique position as part of a fixation artefact. The patent canal running from right to left lies medially adjacent to this thickening (Fig. 4h; "wide" reconstruction). In the ventral aspect of this reconstruction, the epithelial cone forming the ventral opening of the neurenteric canal is visible (Fig. 4i; "wide" reconstruction).

The embryonic disc of the human embryo "Da1" [Ludwig, 1928] chosen to represent stage 9 in this study is sole-shaped and bent into a marked lordosis (Fig. 5b); it measures 2.4 mm in length [Ludwig, 1928]. The presentation of the histological sections (Fig. 5b–d) had to be taken from a printed publication [Ludwig, 1928] with the effect that the cellular borders are difficult to determine. Cranially, the neuroectoderm displays bilaterally symmetrical, broad neural plates while the centre of the embryonic disc

Fig. 5. Human stage 9 embryo (specimen name "Da1"). **a** Dorsal view of a reconstruction in Ludwig [1928] displaying notochord, primitive streak, cut edge of the amnion, proximal parts of the yolk sac, and dorsal opening of the neurenteric canal. B, C, and D indicate the position of transverse sections (images scanned from figures printed in Ludwig [1928] and shown in **b–d** at low (**b**) and high (**c**, **d**) magnification (section numbers are taken from Ludwig [1928] and indicated at the bottom left). Black asterisks mark the border of the embryonic disc. **c** Transverse section cutting the

neurenteric canal longitudinally and thus containing both the dorsal opening (black arrow) and the ventral opening (black arrowhead) of the neurenteric canal. Black circle with line attached marks the hinge of involuting notochord cells in the lateral wall of the neurenteric canal. **d** Transverse section through primitive streak forming the caudal wall of the neurenteric canal. **e** Dorsocaudal view of a "narrow" 3D reconstruction indicating the dorsal opening of the neurenteric canal. Scale bar: **a** 750 μm. **b** 300 μm. **c**, **d** 100 μm.

(For figure see next page.)

section 180

section 183

section 184
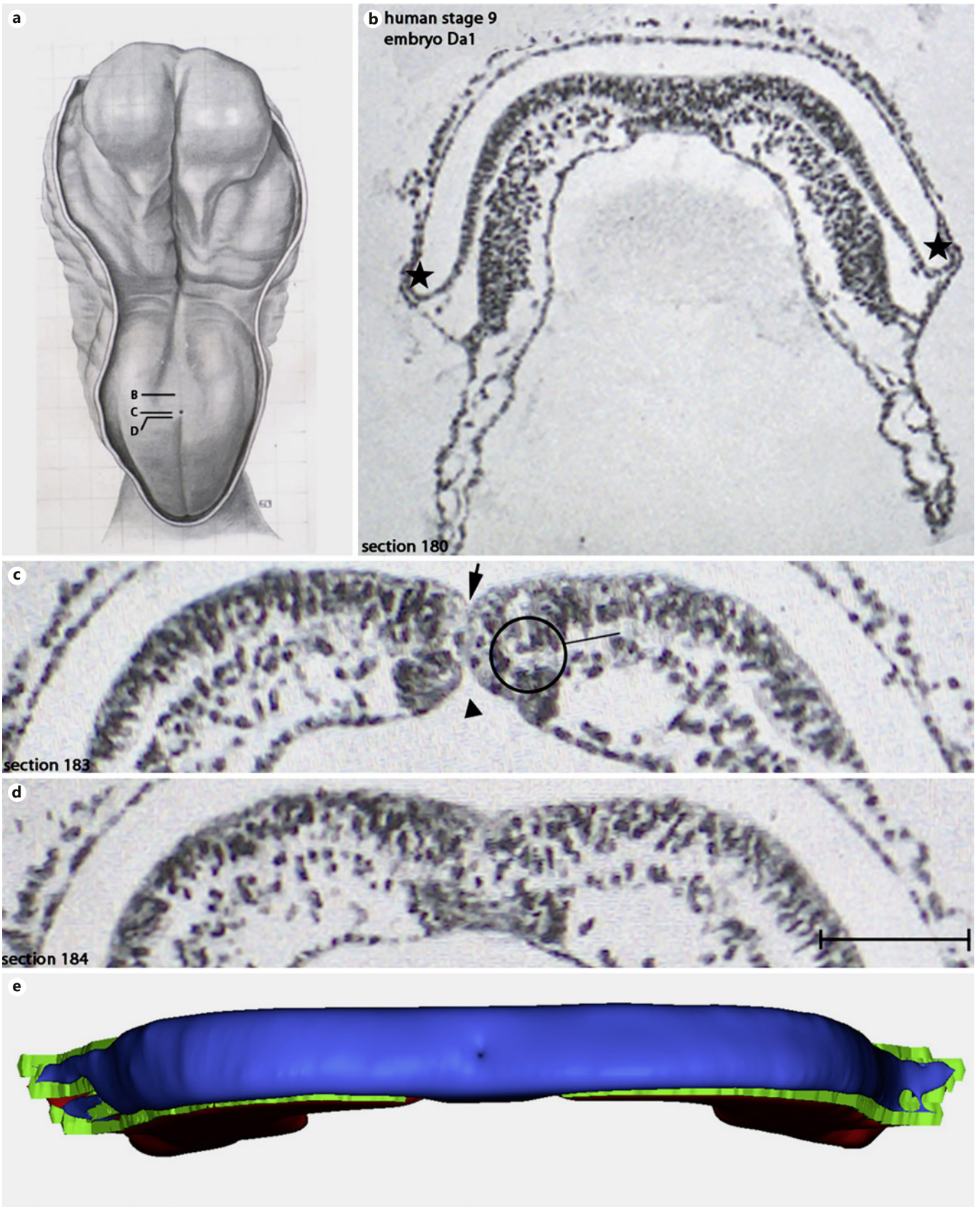
shows elevated neural folds and holds one pair of somites (Fig. 5a). The specimen has a clear perpendicular neurenteric canal immediately anterior to the primitive streak and is limited anteriorly by cells of the floor plate and laterally by the neuroectoderm bent (and representing the node shoulders) around the lateral part of the HINC (Fig. 5c); the HINC is defined by the medial edge of the basement membrane of the neuroectoderm similar to the situation in the specimens of stage 8b described above (Fig. 3, 4). The neuroectoderm thus forms a ventrally oriented cone of epithelium which is continuous with the notochordal plate laterally, cranially (Fig. 5b, c), and also caudally (Fig. 5d); here, a cluster of epithelial cells ventral to the neuroectoderm represents the posterior continuity of the notochordal plate intercalated into the hypoblast in the median plane (Fig. 5d). The walls of the neurenteric canal touch each other in its dorsal half, which gives the canal a narrow appearance. Although similar in shape, the right node shoulder contains more nuclei (and thus more cells) than the left node shoulder (Fig. 5c). The parachordal ectoderm consists of columnar to cuboidal cells and appears symmetrical in shape.

3DR reveals the dorsal opening of the neurenteric canal (Fig. 5e), similar to the original plaster model generated by Ludwig [1928] (Fig. 5a). The neuroectoderm appears symmetrical on both sides of the embryonic disc, which is much like its appearance in the sections.

Morphology of C. jacchus Embryos

Whole-mount views of the stage 8b *Callithrix* embryo made available and dissected for this study (specimen No. GM79.01) reveal an embryonic disc with a neural plate bent ventrally at is cranial and lateral borders to join the epidermal ectoderm, a short allantoic diverticulum, and the cut margins of the yolk sac and the amniotic cavity both of which had been opened peripherally. The whole embryonic disc measures 1.2 × 0.68 mm with the primitive streak marking the posterior (or caudal) one-third, and with a translucent notochordal plate marking the anterior (or cranial) two-thirds of the total length of the anterior-posterior axis (Fig. 6a). In the posterior part of the embryo, at the transition between primitive streak and notochordal plate, the primitive node is visible with a dense left and a less dense right node shoulder, which are connected anterior to the node and together flank an almost translucent primitive pit on both sides. The transverse Technovit® sections reveal the neuroectoderm to be composed of a pseudostratified epithelium with centrally placed cell nuclei and occasional mitotic figures near the apical surface (Fig. 6b–e). Within both node shoulders,

this epithelium bends by 180° around a hinge point which is defined by the medial edge of the neuroectoderm basement membrane and, therefore, is equivalent to the HINC described above in the human embryos (Fig. 1g, 4d, 5c). Lateral to each of these 2 HINCs, the basement membranes separate the notochordal plate underneath from neuroectoderm above. The notochordal plate presents a cuboidal epithelium between the node and the prechordal mesoderm, and is 650 µm long and maximally 140 µm wide immediately anterior to the node. It has direct contact ventrally to the yolk sac cavity and laterally to the paraxial mesoderm, which itself is ventrally covered by a layer of squamous hypoblast cells. Between the 2 HINCs, i.e., in the centre of the primitive node, an oval lumen (40 µm long and 8 µm wide) connects the amniotic cavity and the yolk sac cavity and is, therefore, addressed as a bona fide neurenteric canal as described above for human embryos at stages 8b and 9 (cf. Fig. 5c). In the stereomicroscope, loose cellular debris had been seen to move in and out of the neurenteric canal during handling of the intact yolk sac of this specimen and was found, after embedding, to be trapped in the ventral opening of the neurenteric canal (Fig. 6d). The canal is fully surrounded by a cone of pseudostratified epithelium (Fig. 6c, d) in which cell nuclei are positioned without preference either towards the basement membrane shared with the overlying neuroectoderm or towards the apical surface of the notochordal plate facing the yolk sac cavity. The cranial and lateral two-thirds of this cone are formed by the notochordal plate gently bent from an almost vertical into a horizontal position. Laterally, this cone is attached to the hypoblast (Fig. 6c, d). The caudal part of the cone consists of irregularly arranged epithelial cells (a) of the notochordal plate ventrally, and (b) of the primitive streak (epiblast) dorsally, without clear separation, however, from the more caudal parts of the primitive streak. Next to the entire length of the primitive streak, the ectoderm, mesoderm, and hypoblast layers, and a continuous basement membrane between the first two are easily distinguishable in the paramedian planes; in the median plane, however, the basement membrane is interrupted: ectoderm and mesoderm appear intermingled, and this zone contains cells showing signs of epithelial-mesenchymal transition (Fig. 6e). The cellular architecture of the cone investing the neurenteric canal, therefore, represents signs of cellular involution in its cranial and lateral parts, but not in its caudal part, thereby giving the HINC as a region of involution surrounding the neurenteric canal craniolaterally a horseshoe-like shape. Interestingly, the neuroectodermal epithelium in the right node shoulder (or
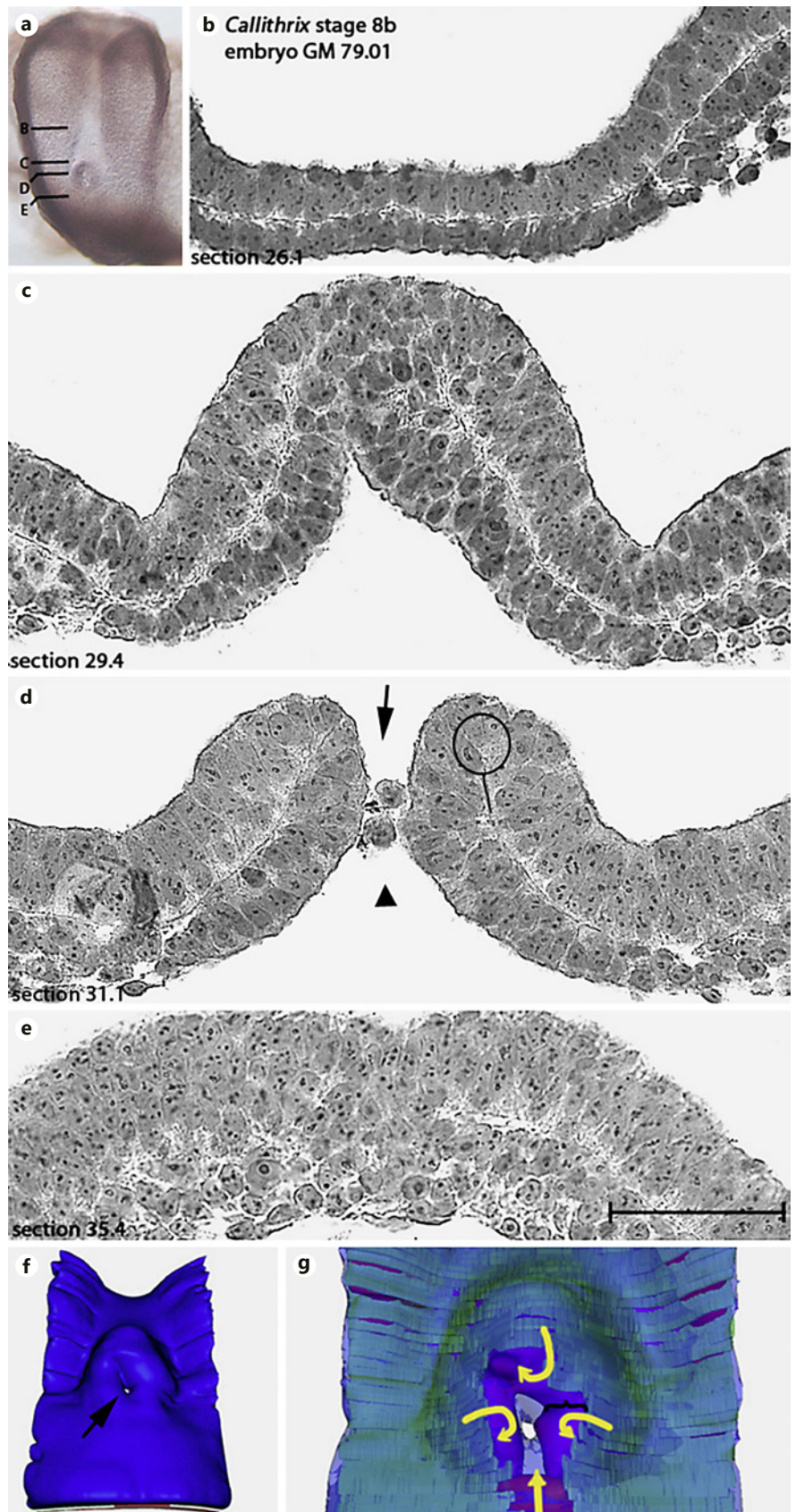
Fig. 6. Callithrix stage 8b embryo (specimen No. GM79.01). **a** Stereomicroscopic dorsal view showing neural plate bulging bilaterally of notochordal process which widens caudally to encompass the dorsal neurenteric canal opening in the primitive node at the junction with the primitive streak (out of focus plane). Cut edge of the yolk sac is seen ventral and lateral to the anterior part of the neural plate. B, C, D, and E indicate the position of the transverse paraffin sections shown in **b–e** (section numbers indicated at the bottom left). **b–e** Transverse sections through the posterior broad part of the notochordal plate (**b**), through the cranial rim of the primitive node (or wall of dorsal neurenteric canal opening) showing lateral asymmetry (**c**), through the centre of the neurenteric canal (transverse arrow and arrowhead marking the dorsal opening and cellular debris within the ventral opening, respectively) with the hinge of involuting notochord cells (HINC; black circle with line attached) in its lateral wall (**d**), and through the cranial part of the primitive streak (**e**). **f** Dorsocaudal view of a "narrow" 3D reconstruction displaying the patent lumen of the neurenteric canal. **g** Enlargement of the semitransparent version of the 3D reconstruction shown in **f** and displaying cranial and medial margins of the basement membrane (green) separating the neuroectoderm and notochordal plate. Curved yellow arrows mark the involution of notochordal cells within the HINC, straight yellow arrow marks the ingression primitive streak mesoderm into the caudal wall of the neurenteric canal. Scale bar: **a** 800 μm. **b–e** 50 μm.

HINC) is slightly higher, and its cellular nuclei are more often round than oval and more often form more layers than in the left node shoulder (or HINC; Fig. 6c, d).

When 3DRs of the primitive node area are tilted and viewed from posterior, the neurenteric canal in the centre of the node is seen to be patent (Fig. 6f). The openings of the almost perpendicular neurenteric canal are connected by small oblique furrows oriented to the anterior left in the dorsal and ventral epithelium for a short distance (Fig. 6f). The right node shoulder is broader than the left and presents itself with a laterally shifted basement membrane forming an oblique oval area composed of ectoderm only (Fig. 6g). The right node shoulder is bent along the circumference of the canal and continues to be the cranial part of the primitive node from which the notochordal plate emerges. Cranial to this elevated part of the primitive node, the embryonic disc shows a broad flat stretch containing the notochordal plate and the floor plate both of which become narrow towards their cranial end (Fig. 6f). Laterally, the embryonic disc is folded and consists of ectoderm, mesoderm, and hypoblast cells as it does in the caudal part, where the lack of a basement membrane in the median plane indicates the position of the primitive streak.

In the stage 9 *Callithrix* embryo (specimen No. GP09.01), the embryonic disc measures 2.1×1.2 mm and is, therefore, slightly larger than the embryonic disc of the stage 8b embryo (GM79.01); the first pair of somites is visible in the paraxial mesoderm under a pear-shaped, flat neural plate, and extraembryonic structures are principally similar to the ones seen in the stage 8b *Callithrix* embryo. The primitive node marks the junction between the primitive streak and a broad notochordal plate as at stage 8a (Fig. 7a), but it rises higher above the neural plate than at stage 8b (not shown) and presents in its centre – in the stereomicroscope and already at low magnification (Fig. 7a) – an oblique canal running from the dorsal caudal right to the ventral cranial left (see below). Transverse histological (paraffin) sections confirm this to be an oval neurenteric canal (20 μm long and 13 μm wide) connecting the yolk sac cavity with the amniotic cavity. As before, the canal lumen is surrounded by an epithelial cone consisting of notochordal plate (Fig. 7d) and primitive streak epiblast (Fig. 7e). The cellular architecture within this cone part of the notochordal plate varies along the craniocaudal axis. Immediately cranial to the neurenteric canal, cells are cuboidal to low columnar with the nuclei positioned towards the basement membrane (Fig. 7b, c), whereas lateral to the neurenteric canal lumen the epithelium is high columnar, and nuclei are positioned in a more irregular fashion (Fig. 7d). Cranial to the neurenteric canal lumen, the neuroectodermal epithelium in the right node shoulder is higher than on the left side (Fig. 7b). Directly caudal to this thickening, the basement membrane on the right side is lacking from the top of the node to its lower third (Fig. 7c). In addition, the cell nuclei within the right node shoulder are almost all round and form up to 5 layers. The nearby area of the primitive streak consists of epiblast, mesoderm, and hypoblast, the first two being intermingled and lacking a medial basement membrane border in the median plane. 3DR visualization confirms the oblique course of the neurenteric canal running from caudodorsal-right to cranioventral-left and being surrounded by epithelial cells. The ventral part of the cone is seen to consist of notochordal cells only (Fig. 7g). Furthermore, in the left node shoulder, the basement membrane rises high towards the dorsal surface (Fig. 7f) which is in contrast to the lack of a basement membrane in the right node shoulder (Fig. 7g).

Asymmetric Nodal *Expression in the Stage 8b* Callithrix *Embryo (Specimen No. GM79.01)*

Besides the morphological asymmetry described above in this embryo (Fig. 6) and using a *Callithrix nodal* cRNA probe, WISH revealed *nodal* expression in the left paraxial mesoderm next to the developing notochordal plate, immediately cranial to the dorsal opening of the neurenteric canal (Fig. 8a); the expression is found in 20 transverse sections further cranially resulting in an expression domain length of 140 μm (Fig. 8a, b). The expression domain ends caudally where the basement membrane of the floor plate shows first discontinuities and forms the horseshoe-shaped HINC in the craniolateral circumference of the primitive node. Although a slight staining reaction on the right side is visible in some sections, this was not strong enough for the purpose of visualizing the asymmetry of the *nodal* expression domains in the 3DR. Thus, 3DR shows the *nodal* domain on the left only, and there is an intimate connection of it with the notochordal plate epithelium (Fig. 8c).

Discussion

Our integrated analysis of modern and historic, human and non-human primate, histological and 3D-reconstructed specimens leads to the unambiguous identification of the neurenteric canal. The cellular components of its wall structures are consistently found in the Hensen's node area and in the axial mesoderm extending
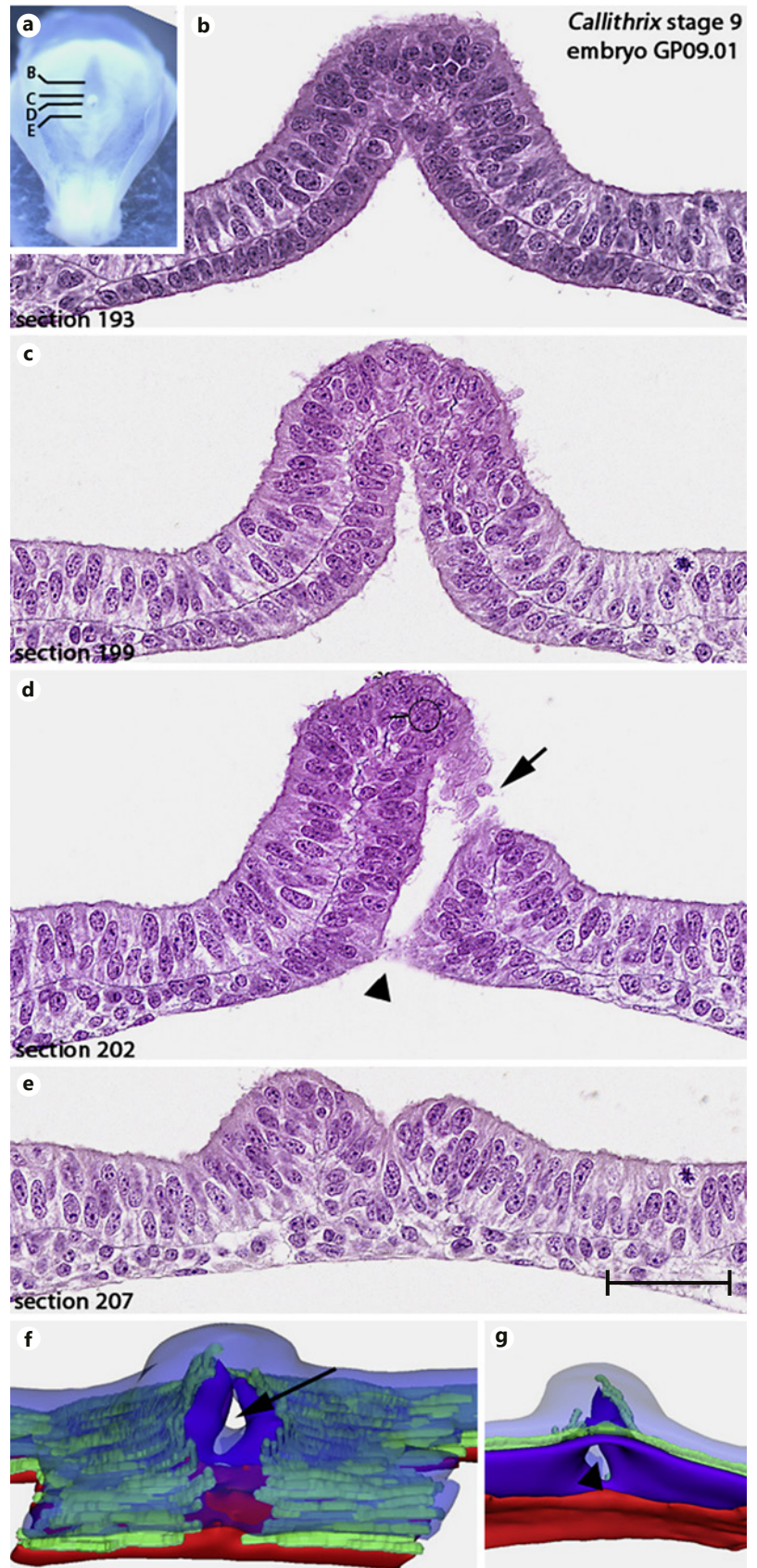
Fig. 7. *Callithrix* stage 9 embryo (specimen No. GP09.01). **a** Stereomicroscopic dorsal view centring on the primitive node at the junction between the broad caudal extremity of the notochordal plate and primitive node. Note dorsal to the neural plate the cut edge of the amnion and caudally the density of the allantois and body stalk, lateral to which is the proximal part of the yolk sac. B–E indicate the position of the transverse Technovit® sections shown in **b–e** (section numbers indicated at the bottom left). **b–e** Sections through the cranial part of the ventral neurenteric canal opening consisting of cuboidal notochordal epithelium (**b**), through the cranial wall of the neurenteric canal with lateral asymmetry (**c**), through the centre of the neurenteric canal (arrow and arrowhead marking the cranial part of the dorsal opening wall and the caudal part of the ventral opening wall, respectively) with the hinge of involuting notochord cells (black circle with line attached) in its lateral wall (**d**), and through the cranial part of the primitive streak forming the caudal wall of the ventral neurenteric canal opening (**e**). **f** Dorsocaudal view of a semitranslucent version of a "narrow" 3D reconstruction displaying the patent lumen of the neurenteric canal (arrow marking the dorsal opening of the neurenteric canal). Colour coding as in Figure 9g. **g** Ventrocranial view of a "narrow" semitranslucent 3D reconstruction (arrowhead marking the ventral opening of the neurenteric canal). Scale bar: **a** 1 mm. **b–e** 50 μm.

Fig. 8. Asymmetric *nodal* expression in a *Callithrix* stage 8b embryo (specimen No. GM79.01). **a** Stereomicroscopic caudodorsal view centering on the primitive node containing the dorsal opening of the neurenteric canal. Arrow marks left *nodal* expression at the lateral border of the broad posterior part of the notochordal plate. **b** Transverse section (number indicated at the bottom left) through the centre of the *nodal* domain (arrow) in parachordal cells and basal parts of overlying neuroectodermal cells at the left margin of the notochordal plate. Note weak colour reaction in parachordal cells and overlying neuroectodermal cells at the right notochordal plate margin. **c** Caudodorsal view of semitranslucent "narrow" 3D reconstruction. Colour coding similar to Figure 9 except for *nodal* domain (dark green). Scale bar: **a** 220 μm. **b** 100 μm. **c** 180 μm.

from it in late pre-somite (Carnegie stage 8) and early somite stage (Carnegie stage 9) human embryos and this is schematically represented in Fig. 9c. At early and late stages 8 the cellular components of the near-midline neuroectoderm, axial mesoderm, and primitive streak determine the size of the (newly defined) radially expanding HINC in Hensen's node to form the notochordal canal as a forerunner structure to the neurenteric canal (schematically represented in Fig. 9a, b). The SCM has a central position in the transition from notochordal canal to neurenteric canal and its analysis may now form the basis for finding mechanisms of neurenteric canal formation and for inborn pathologies of axial structures seen in the newborn and in early childhood.

Distinction of Neurenteric and Notochordal Canals and the Evolution of Amniote Gastrulation

The histological findings and high-resolution 3DRs of the stage 8b and the stage 9 *C. jacchus* embryos presented here were crucial in identifying the cellular architecture of the notochordal canal and the neurenteric canal in the human embryo of equivalent stages. Applying this histological information to the published data on the few relevant human specimens available worldwide leaves little doubt about the neurenteric canal being a regular but short-lived feature in the human. It is formed at the late stage 8 by local dissolution of the SCM and then shows transient patency at the early stage 9. The ventrally oriented funnel-shape opening lined by a cone of epithelial cells can now be recognized by the arrangement of nuclei near the ventral opening also in badly fixed specimens such as embryo Gle [von Spee, 1889], Peh.1 [Rossenbeck, 1923], and R.S. [Odgers, 1941] for late stage 8 or embryo H3 [Wilson, 1914] for stage 9, respectively. The fact that the new excellently preserved human early-stage-8 embryo presented here had been sectioned sagittally offered the rare chance, in addition, to verify the features of a hinge-like involution present in the 2 sagittally sectioned human stage 8 embryos of which median notochord histology had been published previously: in embryo CC8671 (Fig. 5) [Hertig, 1968; Fig. 106] and in embryo CC7972 [Müller and O'Rahilly, 2003, Fig. 4; cf. O'Rahilly and Müller, 1987, Appendix I].

High-resolution histological analysis complemented with 3DR applied to 3 consecutive stages (stages 8a, 8b, and 9) reinforced, then, the classical distinction between the notochordal and the neurenteric canal [Grosser, 1924] and the formation of the latter from the former [O'Rahilly and Müller, 1987] by dissolution of the SCM, which forms the ventral wall of the notochordal canal at
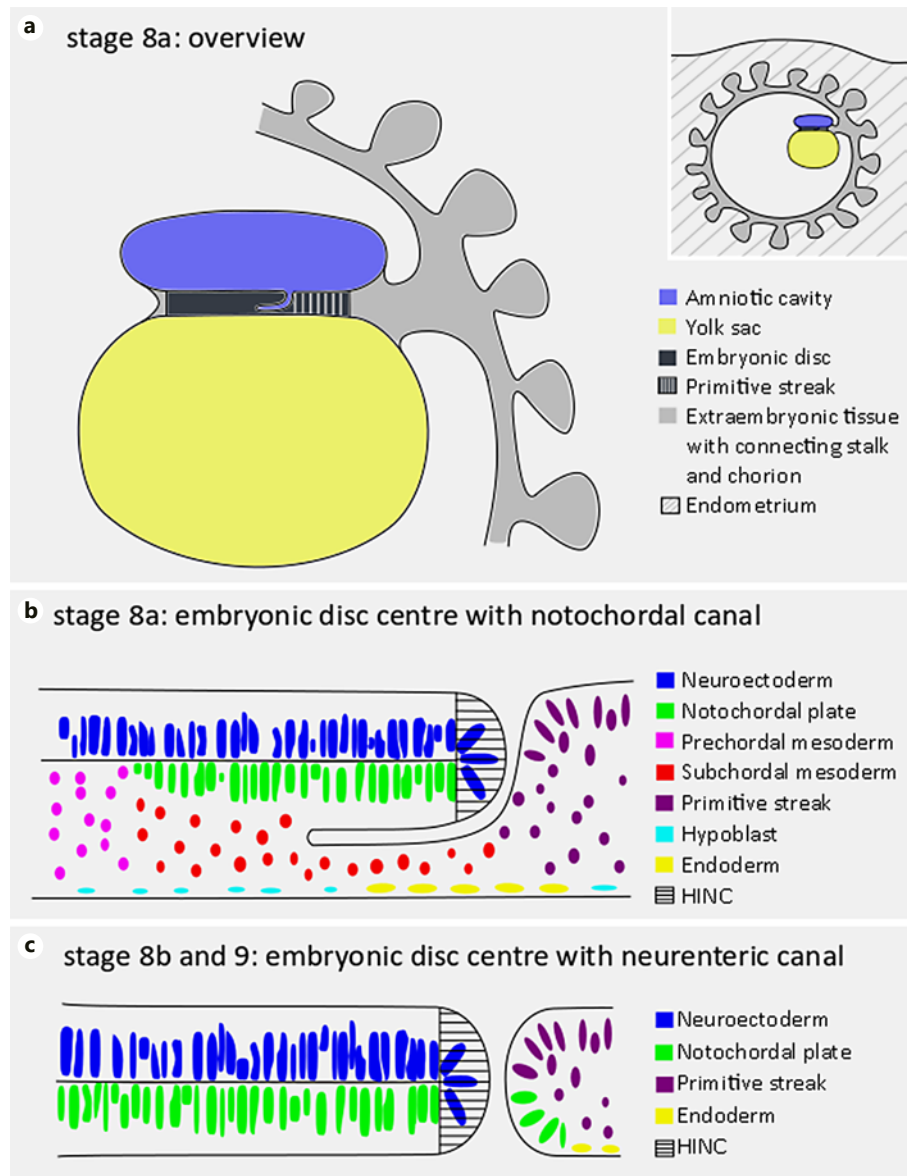
Fig. 9. Schematic drawing of median sagittal sections illustrating the topography of the notochordal canal and the neurenteric canal in the human embryo. **a** Overview at stage 8a with the amniotic cavity (light blue), yolk sac (light yellow), embryonic disc (black), and extraembryonic mesoderm, body stalk, and chorion (grey) as placed in the endometrium (inset) as part of the interstitial implantation of the conceptus. The notochordal canal has a dorsal connection to the amniotic cavity, only. **b** Detailed view at stage 8a illustrating the cellular composition of the notochordal canal wall and adjacent tissues. Coloured shapes represent cellular nuclei (see colour coding legend). **c** Detailed view of stage 8b illustrating the cellular composition of the neurenteric canal wall and adjacent tissues. Colour coding as in **b**. Note notochordal plate cells surrounding the ventral opening of the neurenteric canal. HINC, hinge of involuting notochord cells.

its caudal-most part immediately cranial to the primitive node. The definition of the notochordal plate as an epithelial part of the axial mesoderm presented here is more encompassing than the original description of the notochordal plate given by O'Rahilly and Müller [1981] who saw the notochordal plate confined to the central part of the developing notochord transiently intercalated into the endoderm and thereby exposed to the yolk sac cavity. In the light of previous descriptions provided by Selenka [1900] on the mangabey and gibbon, which are in accordance with studies on baboon and macaque embryos [Hendrickx, 1971; Heuser and Streeter, 1941;

Tamarin, 1983] where the dorsal opening of a possible neurenteric canal is documented, the cranial and craniolateral walls of the dorsal opening of the notochordal (and later neurenteric) canal are now defined as the horseshoe-shaped HINC and a universal characteristic of primate and reptile embryogenesis. Considering early morphological studies [Kowalevsky, 1877; Hoffmann, 1883; van Beneden, 1888], it seems justified to renew and refine the hypothesis that the mammalian neurenteric canal – together with the cranially adjacent HINC within the Hensen node – is homologous to the blastopore as a whole in reptiles and to the dorsal segment of

the blastopore with its adjacent blastoporal lips in amphibia: both the neurenteric canal and the blastopore are in their cranial part associated with an involution-type cell movement for the formation of the notochordal plate, and this shows striking parallels in primates [this study], bats [van Beneden, 1888], reptiles [Bertocchini et al., 2013; Stower and Bertocchini, 2017], amphibia [Shook and Keller, 2008], and in a number of bird species (including the chick: Charrier et al. [1999]; Tsikolia et al. [2012]), some of which may also have a notochordal canal ("rudimentary Urdarm") or even a true neurenteric canal [Schauinsland, 1903]; in the chick, however, a neurenteric canal next to the HINC-like cellular arrangement within the primitive node [Tsikolia et al., 2012] has not yet been reported. The primitive streak itself would, hence, represent a homologue of the lateral and ventral parts of the blastopore as described before (see Hertwig [1906] and references therein). Intriguingly, reptiles – and possibly some rare avian species [cf. Schauinsland, 1903] – may thus be suitable to serve as a new model organism for notochord development and neurulation (see below) in primates, in particular. Finally, the primarily asymmetrical *nodal* expression in the stage 8 *Callithrix* embryo together with morphological asymmetries in the node suggests that primates make use of an early non-cilium-dependent left-right symmetry breaking mode similar to the situation in the chick, pig, and cattle [Schröder et al., 2016].

Intriguingly, the SCM seems to play a transient structural role in 2 processes central to gastrulation which have hitherto not been described to be functionally related: In many amniotes, the SCM covers up the potentially cilium-carrying apical surface of the notochord at the phase when the axial mesoderm forms a barrier to maintain early molecular left-right asymmetry [Blum et al., 2014; Schröder et al., 2016], and in primates the SCM seems to be centrally positioned for the formation of the neurenteric canal, which is, in turn, a central structure of the axial mesoderm. Experimental comparative analysis of the mechanism involved in origin, fate, and molecular characteristics of the SCM in the chick, mouse, and pig, for example, seems now to be a rewarding enterprise to clarify several processes central to gastrulation, neurulation, and establishing the amniote body plan.

The Neurenteric Canal and Embryonic Malformations

A proper spatial understanding of the formation of the neurenteric canal is also important when considering its possible role in congenital malformations because the neurenteric canal is located at the transition from primary to secondary neurulation albeit as a temporary connection only between the amniotic cavity and primitive gut: The area undergoing secondary neurulation posterior to the neurenteric canal has to fuse with the neural tube and the notochord formed during primary neurulation. The persistent neurenteric canal may cause defects in this fusion which has been recently described as defects of the so-called junctional neurulation [Dady et al., 2014; Eibach et al., 2017; Schmidt et al., 2017; Florea et al., 2018]. Furthermore, the neurenteric canal may allow the migration of multipotent endodermal cells producing neuroendodermal cysts (or neurenteric cysts in the old nomenclature of de Oliveira et al. [2005]) along the entire neuroaxis including the supratentorial space (the cavity cranial to the cerebellum) in infants and middle-aged adults [Mittal et al., 2010]. These cysts can grow enormously in a short time [Priamo et al., 2011], causing neurological symptoms such as paraplegia [Rizk et al., 2001] and the need for neurosurgical intervention with close diagnostic follow-up by magnetic resonance imaging [Yang et al., 2015]. The neurenteric canal has also been suggested to be involved in the development of rare but severe abnormalities summarized as the split notochord syndrome which includes dorsal enteric fistula, a split vertebral column, and intestinal alterations [Bentley and Smith, 1960; Holschneider and Fendel, 1971; Singh and Singh, 1982; Gupta and Deodhar, 1987; Dhawan et al., 2017]. The thoracolumbar transition zone as the level where these deformities occur corresponds to the area impaired should a neurenteric canal persist beyond stage 10, and, indeed, experimental studies using the newt *Cynopus pyrrhogaster* proved that the split notochord syndrome can be mechanically induced here [Emura et al., 2000, 2003]. The level of the deformities observed also played a role in the dismissal [Hueston, 1953] of the suggestion that a sacrococcygeal fistula (also called pilonidal sinus) may originate from the persistent neurenteric canal [Kallet, 1940]: a pilonidal sinus arises principally at the sacrococcygeal level and, apart from this, does not involve intestinal tissue. A more likely hypothesis is, therefore, that pilonidal sinuses originate from the caudal part of the neural cord, which forms by secondary neurulation [cf. O'Rahilly and Mueller, 2001]. Further research, especially a high-resolution histological re-examination of at least all 31 remaining human stage 8 and 9 embryos of the Carnegie Collection [O'Rahilly and Müller, 1987; Appendix I] and of selected new pre-somite *Callithrix* embryos, may now substantiate these concepts and, some day, help the understanding of the molecular pathways leading to these malformations.

Rulle/Tsikolia/de Bakker/Drummer/Behr/
Viebahn

Acknowledgements

The authors would like to thank Kirsten Falk-Stietenroth, Hannes Sydow, Heike Faust, and Irmgard Weiss for their technical assistance, Dr. Henny van Straaten (Maastricht), pioneer in experimental studies of the chick notochord, for valuable discussions and his help in assembling and annotating a complete list of published human embryos with signs of a neurenteric canal, Dr. Peter Giere (Berlin) for his support in photographing the embryo Dobbin, John Cork, Ph.D and Raymond F. Gasser, PhD (New Orleans) for the images of the embryo CC10157, Dr. Katharina Debowski (Göttingen) for supplying the *Callithrix nodal* probe, Angelina Berenson and Nicole Umland for assistance in animal work, Dr. Matthias Ochs (Berlin) and Dr. Wolfgang Knabe (Münster) for valuable discussions on 3DR issues.

References

Aeckerle, N., C. Drummer, K. Debowski, C. Viebahn, R. Behr (2015) Primordial germ cell development in the marmoset monkey as revealed by pluripotency factor expression: suggestion of a novel model of embryonic germ cell translocation. Mol Hum Reprod *21:* 66–80.

Arendt, D., K. Nübler-Jung (1999) Rearranging gastrulation in the name of yolk. Evolution of gastrulation in yolk-rich amniote eggs. Mech Dev *81:* 3–22.

Bancroft, J.D., C. Layton (2013) The hematoxylin and eosin; in Suvarna, S.K., C. Layton, J.D. Bancroft (eds): Bancroft's Theory and Practice of Histological Techniques. Churchill Livingstone Elsevier.

Beck, C.W., J.M.W. Slack (1998) Analysis of the developing *Xenopus* tail bud reveals separate phases of gene expression during determination and outgrowth. Mech Dev *72:* 41–52.

Bentley, J.F.R., J.R. Smith (1960) Developmental posterior enteric remnants and spinal malformations: the split notochord syndrome. Arch Dis Child *35:* 76–86.

Bertocchini, F., C. Alev, Y. Nakaya, G. Sheng (2013) A little winning streak: the reptilian-eye view of gastrulation in birds. Dev Growth Differ *55:* 52–59.

Blum, M., A. Schweickert, P. Vick, C.V.E. Wright, M.V. Danilchik (2014) Symmetry breakage in the vertebrate embryo. When does it happen and how does it work? Dev Biol *393:* 109–123.

Boroviak, T., R. Loos, P. Lombard, J. Okahara, R. Behr, E. Sasaki, et al. (2015) Lineage-specific profiling delineates the emergence and progression of naive pluripotency in mammalian embryogenesis. Dev Cell *35:* 366–382.

Cambray, N., V. Wilson (2002) Axial progenitors with extensive potency are localised to the mouse chordoneural hinge. Development *129:* 4855–4866.

Charrier, J.-B., M.-A. Teillet, F. Lapointe, N.M. Le Douarin (1999) Defining subregions of Hensen's node essential for caudalward movement, midline development and cell survival. Development *126:* 4771–4783.

Cork, J.R., R.F. Gasser (2017a) Virtual human embryo project. http://virtualhumanembryo.lsuhsc.edu/downloads/DREM_disks.html (accessed October 2018).

Cork, J.R., R.F. Gasser (2017b) Introduction – virtual human embryo project. http://virtualhumanembryo.lsuhsc.edu/demos/Stage8_v2/Intro_pg/Intro.htm (accessed October 2018).

Cork, J.R., R.F. Gasser (2017c) Browse sections – virtual human embryo project. http://virtualhumanembryo.lsuhsc.edu/demos/Stage8_v2/Brws_pg/Disp_FS.htm (accessed October 2018).

Dady, A, E. Havis, V. Escriou, M. Catala, J.-L. Duband (2014) Junctional neurulation. A unique developmental program shaping a discrete region of the spinal cord highly susceptible to neural tube defects. J Neurosci *34:* 13208–13221.

de Bakker, B.S., K.H. de Jong, J. Hagoort, K. de Bree, C.T. Besselink, F.E.C. de Kanter, et al. (2016) An interactive three-dimensional digital atlas and quantitative database of human development. Science *354:* aag0053.

de Oliveira, R.S., G. Cinalli, T. Roujeau, C. Sainte-Rose, A. Pierre-Kahn, M. Zerah (2005) Neurenteric cysts in children: 16 consecutive cases and review of the literature. J Neurosurg *103:* 512–523.

Debowski, K., C. Drummer, J. Lentes, M. Cors, R. Dressel, T. Lingner, et al. (2016) The transcriptomes of novel marmoset monkey embryonic stem cell lines reflect distinct genomic features. Sci Rep *6:* 29122.

Dhawan, V., K. Kapoor, B. Singh, S. Kochhar, A. Sehgal, R. Dada (2017) Split notochord syndrome. A rare variant. J Pediatr Neurosci *12:* 177–179.

Eibach, S., G. Moes, Y.J. Hou, J. Zovickian, D. Pang (2017) Unjoined primary and secondary neural tubes: junctional neural tube defect, a new form of spinal dysraphism caused by disturbance of junctional neurulation. Childs Nerv Syst *33:* 1633–1647.

Emura, T., M. Asashima, K. Hashizume (2000) An experimental animal model of split cord malformation. Pediatr Neurosurg *33:* 283–292.

Emura, T., K. Hashizume, M. Asashima (2003) Experimental study of the embryogenesis of gastrointestinal duplication and enteric cyst. Pediatr Surg Int *19:* 147–151.

Eternod, A. C. F. (1899) Il y a un canal notochordal dans l'embryon humain. Anat Anz *16:* 131–143.

Florea, S.M., A. Faure, H. Brunel, N. Girard, D. Scavarda (2018) A case of junctional neural tube defect associated with a lipoma of the filum terminale: a new subtype of junctional neural tube defect? J Neurosurg Pediatr *21:* 601–605.

Gihr, M. (1961) Methode zur Rekonstruktion von Nervenzellen. J Hirnforsch *5:* 7–22.

Gilbert, S.F., M.J.F. Barresi (2016) Developmental Biology, ed 11. Sunderland, Sinauer Associates Inc.

Gont, L.K., H. Steinbeisser, B. Blumberg, E.M. de Robertis (1993) Tail formation as a continuation of gastrulation. The multiple cell populations of the *Xenopus* tailbud derive from the late blastopore lip. Development *119:* 991.

Greenough, T.C., A. Carville, J. Coderre, M. Somasundaran, J.L. Sullivan, K. Luzuriaga, K. Mansfield (2005) Pneumonitis and multiorgan system disease in common marmosets (*Callithrix jacchus*) infected with the severe acute respiratory syndrome-associated coronavirus. Am J Pathol *167:* 455–463.

Grosser, O. (1924) Junge menschliche Embryonen (der dritten und vierten Woche). Erg Anat Entw Gesch *25:* 390–447.

Gupta, D.K., M.C. Deodhar (1987) Split notochord syndrome presenting with meningomyelocoele and dorsal enteric fistula. J Pediatr Surg *22:* 382–383.

Haeckel, E. (1874) Die Gastraea-Theorie, die Phylogenetische Classification des Tierreichs und die Homologie der Keimblatter. Jena Z Naturw *8:* 1–55.

Hendrickx, A.G. (1971) Embryology of the Baboon. Chicago, University of Chicago Press.

Hensen, V. (1876). Beobachtungen über die Befruchtung und Entwicklung des Kaninchens und Meerschweinchens. Z Anat Entwickl Gesch *1:* 213-273, 353–423.

Hertig, G. (1968) Human Trophoblast. Springfield, Ill., Thomas.

Hertig, G., H. Gore (1966) The female genitalia. Placenta, Amnion and Umbilical Cord; in Anderson, W.A.D.: Pathology, ed 5. St. Louis, Mosby.

Hertwig, O. (1906) Lehrbuch der Entwicklungsgeschichte des Menschen und der Wirbeltiere, Band 1, Teil 1, pp 699–966. Jena, Fischer.

Heuser, C.H. (1932) A presomite human embryo with a definite chorda canal. Contrib Embryol *23:* 251–267.

Heuser, C.H., G.L. Streeter (1941) Development of the macaque embryo. Contrib Embryol *29:* 15.

Hill, J.P., J. Florian (1931) A young human embryo (embryo Dobbin) with head-process and prochordal plate. Philos Trans R Soc Lond B Biol Sci *219:* 443–486.

Hoffmann, C.K. (1883) Zur Ontogenie der Knochenfische. Arch Mikrosk Anat *23:* 45–108.

Holschneider, A.M., H. Fendel (1971) Beitrag zu Wirbelsäulenfehlbildungen in Kombination mit intestinalen und urogenitalen Missbildungen. Z Kinderchir *10:* 230–238.

Hueston, J.T. (1953) The aetiology of pilonidal sinuses. Br J Surg *41:* 307–311.

Kallet, H.I. (1940) Pilonidal sinus. Am J Surg *50:* 648–652.

Kowalevsky, A. (1877) Weitere Studien über die Entwicklungsgeschichte des *Amphioxus lanceolatus*, nebst einem Beitrage zur Homologie des Nervensystems der Würmer und Wirbelthiere. Arch Mikrosk Anat *13:* 181–204.

Leibovitch, E., J.E. Wohler, M. Cummings, M. Sheila, K. Motanic, E. Harberts, M.I. Gaitán, et al. (2013) Novel marmoset (*Callithrix jacchus*) model of human herpesvirus 6A and 6B infections. Immunologic, virologic and radiologic characterization. PLoS Pathog *9:* e1003138.

Lieberkühn, N. (1882) Über die Chorda bei Säugethieren. Arch Anat Entw Gesch, pp 399–438.

Ludwig, E. (1928) Über einen operativ gewonnen menschlichen Embryo mit einem Ursegemente. Gegenbaurs Morphol Jahrb *59:* 41–103.

Mittal, S., K. Petrecca, A.J. Sabbagh, M. Rayes, D. Melançon, M.-C. Guiot, A. Olivier (2010) Supratentorial neurenteric cysts – a fascinating entity of uncertain embryopathogenesis. Clin Neurol Neurosurg *112:* 89–97.

Müller, F., R. O'Rahilly (2003) The prechordal plate, the rostral end of the notochord and nearby median features in staged human embryos. Cells Tissues Organs *173:* 1–20.

Müller, F., R. O'Rahilly (2004) The primitive streak, the caudal eminence and related structures in staged human embryos. Cells Tissues Organs *177:* 2–20.

Neuhauser, E.B.D., H.J. Kaufmann (1961) A.O. Kovalevski and the neurenteric canal. A note on some historical inaccuracies. Proc R Soc Med *54:* 927–929.

Odgers, P.N.B. (1941) A presomite human embryo with a neurenteric canal (embryo R.S.). J Anat *75:* 381–388.3.

O'Rahilly, R., F. Müller (1981) The first appearance of the human nervous system at stage 8. Z Anat Entw Gesch *163:* 1–13.

O'Rahilly, R., F. Müller (1987) Development Stages in Human Embryos. Washington, Carnegie Institution of Washington.

O'Rahilly, R., F. Müller (2001) Human Embryology and Teratology. New York, Wiley-Liss.

O'Rahilly, R., F. Müller (2006) The Embryonic Human Brain. An Atlas of Developmental Stages, ed 3. Hoboken, Wiley.

Pasteels, J. (1943) Proliférations et croissance dans la gastrulation et la formation de la queue des vertébrés. Arch Biol *54:* 1–51.

Priamo, F.A.I., E.D. Jimenez, E.A. Benardete (2011) Posterior fossa neurenteric cysts can expand rapidly: case report. Skull Base Rep *1:* 115–124.

Püschel, B., A. Jouneau (2015) Whole-mount in situ hybridization to assess advancement of development and embryo morphology. Methods Mol Biol *1222:* 255–265.

Rizk, T., G.A. Lahoud, J. Maarrawi, R. Hourani, P. Jabbour, S. Koussa, N. Okais (2001) Acute paraplegia revealing an intraspinal neurenteric cyst in a child. Childs Nerv Syst *17:* 754–757.

Rossenbeck, H. (1923) Ein junges menschliches Ei. Ovum humanum Peh.1 - Hochstetter. Z Anat Entwickl Gesch *68:* 325–385.

Sander, I. (2001) Beschreibung eines menschlichen Embryos der dritten Woche; Thesis Medical Faculty, University of Göttingen.

Sasaki, E., K. Hanazawa, R. Kurita, A. Akatsuka, T. Yoshizaki, H. Ishii, et al. (2005) Establishment of novel embryonic stem cell lines derived from the common marmoset (*Callithrix jacchus*). Stem Cells *23:* 1304–1313.

Schauinsland, H.H. (1903) Beiträge zur Entwicklungsgeschichte und Anatomie der Wirbeltiere. Stuttgart, Nägele.

Schindelin, J., I. Arganda-Carreras, E. Frise, V. Kaynig, M. Longair, T. Pietzsch, et al. (2012) Fiji: an open-source platform for biological-image analysis. Nat Methods *9:* 676–682.

Schmidt, C., V. Voin, J. Iwanaga, F. Alonso, R.J. Oskouian, N. Topale, et al. (2017) Junctional neural tube defect in a newborn. Report of a fourth case. Childs Nerv Syst *33:* 873–875.

Schröder, S.S., N. Tsikolia, A. Weizbauer, I. Hue, C. Viebahn (2016) Paraxial nodal expression reveals a novel conserved structure of the left-right organizer in four mammalian species. Cells Tissues Organs *201:* 77–87.

Selenka, E. (1900) Studien über Entwickelungsgeschichte der Tiere. Wiesbaden, Kreidel.

Shook, D.R., R. Keller (2008) Epithelial type, ingression, blastopore architecture and the evolution of chordate mesoderm morphogenesis. J Exp Zool B Mol Dev Evol *310:* 85–110.

Singh, A., R. Singh (1982) Split notochord syndrome with dorsal enteric fistula. J Pediatr Surg *17:* 412–413.

Sternberg, H. (1927) Beschreibung eines menschlichen Embryos mit vier Ursegmentpaaren. Z Anat Entw Gesch *82:* 142–240.

Stower, M.J., F. Bertocchini (2017) The evolution of amniote gastrulation. The blastopore-primitive streak transition. Wiley Interdiscip Rev Dev Biol *6:* e262.

Strahl, H. (1916) Über einen jungen menschlichen Embryo nebst Bemerkungen zu C. Rabl's Gastrulationstheorie. Anat Hefte *54:* 13–147.

Tamarin, A. (1983) Stage 9 macaque embryos studied by scanning electron microscopy. J Anat *137:* 765.

Thomson, J.A., J. Kalishman, T.G. Golos, M. Durning, C.P. Harris, J.P. Hearn (1996) Pluripotent cell lines derived from common marmoset (*Callithrix jacchus*) blastocysts. Biol Reprod*55:* 254–259.

Tsikolia, N., S. Schröder, P. Schwartz, C. Viebahn (2012) Paraxial left-sided nodal expression and the start of left-right patterning in the early chick embryo. Differentiation *84:* 380–391.

van Beneden, É. (1888) Untersuchungen über die Blätterbildung, den Chordakanal und die Gastrulation bei den Säugetieren, Kaninchen und Vespertilio murinus betreffend. Anat Anz *3:* 709–714.

von Spee, F. (1889) Beobachtungen an einer menschlichen Keimscheibe mit offener Medullarrinne und Canalis neurentericus. Arch Anat Physiol, pp 159–176.

Wilson, J.T. (1914) Observations upon young human embryos. J Anat Physiol *48:* 315–351.

Yang, T., L. Wu, J. Fang, C. Yang, X. Deng, Y. Xu (2015) Clinical presentation and surgical outcomes of intramedullary neurenteric cysts. J Neurosurg Spine *23:* 99–110.